Cancer cells differentially modulate mitochondrial respiration to alter redox state and enable biomass synthesis in nutrient-limited environments

Sarah M. Chang[1,2,3], Muhammad Bin Munim[1,2], Sonia E. Trojan[1,4], Huel Cox III[1,3,], Anna Shevzov-Zebrun[1,2], Keene L. Abbott[1,2], Renee Chang[1,2], and Matthew G. Vander Heiden[1,2,5*]

[1]Koch Institute for Integrative Cancer Research, Massachusetts Institute of Technology, Cambridge, MA, USA

[2]Department of Biology, Massachusetts Institute of Technology, Cambridge, MA, USA

[3]Harvard/MIT MD-PhD Program, Boston, MA, USA

[4]Jagiellonian University Medical College, Faculty of Medicine, Chair of Medical Biochemistry, Krakow, Poland

[5]Dana-Farber Cancer Institute, Boston, MA, USA

*Correspondence: mvh@mit.edu

Abstract

The cell NAD+/NADH ratio can constrain biomass synthesis and influence proliferation in nutrient-limited environments. However, which cell processes regulate the NAD+/NADH ratio is not known. Here, we find that some cancer cells elevate the NAD+/NADH ratio in response to serine deprivation by increasing mitochondrial respiration. Cancer cells that elevate mitochondrial respiration have higher serine production and proliferation in serine limiting conditions than cells with no mitochondrial respiration response, independent of serine synthesis enzyme expression. Increases in mitochondrial respiration and the NAD+/NADH ratio promote serine synthesis regardless of whether serine is environmentally limiting. Lipid deprivation can increase the NAD+/NADH ratio via mitochondrial respiration in some cells, including cells that do not increase respiration following serine deprivation. Thus, in cancer cells where lipid depletion raises the NAD+/NADH ratio, proliferation in serine depleted environments improves when lipids are also depleted. Taken together, these data suggest that changes in mitochondrial respiration in response to nutrient deprivation can influence the NAD+/NADH ratio in a cell-specific manner to impact oxidative biomass synthesis and proliferation. Given the complexity of tumor microenvironments, this work provides a metabolic framework for understanding how levels of more than one environmental nutrient affect cancer cell proliferation.

Introduction

Rapidly proliferating cells, including cancer cells, must acquire biomass precursors such as amino acids, lipids, and nucleotides to support cell growth and division (Deberardinis, 2008; Faubert, 2020; Hanahan, 2011; Pavlova, 2017; Vander Heiden, 2017). While cells can obtain biomass precursors from the environment, many tissue and tumor environments can be deficient in necessary nutrients (Cognet, 2024; Gullino, 1964; Lyssiotis, 2017). In these conditions, cells depend on synthesis pathways to accumulate sufficient biomass for proliferation (Apiz Saab, 2023; Ferraro, 2021; Ngo, 2020; Sciacovelli, 2022; Sullivan, 2019b; Sullivan, 2019a). Synthesis of many

49 biomass precursors involve oxidation reactions that require the redox cofactor NAD+ to act as an
50 electron acceptor. There is accumulating evidence that NAD+ availability and the cell redox state
51 (NAD+/NADH ratio) can limit the synthesis of biomass precursors, including aspartate (Birsoy,
52 2015; Sullivan, 2015), asparagine (Krall, 2021), fatty acids (Li, 2022), serine (Baksh, 2020; Bao,
53 2016; Broeks, 2023; Diehl, 2019), and nucleotides (Bao, 2016; Diehl, 2019; Wu, 2024). Thus, the
54 NAD+/NADH ratio impacts cancer cell proliferation in nutrient environments that increase
55 dependence on biosynthetic oxidation reactions. However, what determines the cell NAD+/NADH
56 ratio and whether the NAD+/NADH ratio is modulated in response to environmental nutrient
57 availability is not well characterized. Moreover, whether differences in the NAD+/NADH ratio
58 across cell types affect sensitivity to different nutrient limitations is not known.

59 Some tumor microenvironments have low levels of serine, an amino acid used to produce
60 many biomass components, including proteins, nucleotides, glutathione, and lipids. Thus, low
61 serine environments can limit cancer cell proliferation and tumor growth (Banh, 2020; Maddocks,
62 2013; 2017; Ngo, 2020; Sullivan, 2019b). In serine depleted environments, cancer cells must
63 increase serine synthesis to maintain proliferation (DeNicola, 2015; Labuschagne, 2014;
64 Locasale, 2011; Possemato, 2011; Sullivan, 2019b). Serine synthesis involves the conversion of
65 the glycolytic intermediate 3-phosphoglycerate (3-PG) into serine. The production of 3-PG from
66 glucose involves an oxidation reaction catalyzed by glyceraldehyde 3-phosphate dehydrogenase
67 (GADPH). 3-PG is then oxidized by phosphoglycerate dehydrogenase (PHGDH) in the first step
68 of the serine synthesis pathway. Both GADPH and PHGDH require NAD+ as an electron acceptor
69 to enable serine synthesis. Experimentally blunting NAD+ regeneration from NADH reduces
70 serine synthesis and is rescued by oxidizing the NAD+/NADH ratio via exogenous electron
71 acceptor supplementation (Bao, 2016; Diehl, 2019; Gravel, 2014). Similarly, de novo fatty acid
72 synthesis can be constrained by the NAD+/NADH ratio, as the production of fatty acids involves
73 multiple oxidation reactions to generate citrate from either glucose or glutamine. Thus, decreasing
74 the NAD+/NADH ratio sensitizes cells to environmental lipid depletion (Li, 2022). Together, these

75 findings demonstrate that exogenous changes to the NAD+/NADH ratio can alter serine and
76 citrate production and impact proliferation in serine- or lipid-depleted environments. However,
77 auxotrophy for a single nutrient is not sufficient to determine whether cancer cells can form tumors
78 in a tissue, where levels of variable nutrients may be environmentally limiting for proliferation
79 (Abbott, 2026; Sivanand, 2024; Sullivan, 2019a).Thus, we aimed to uncover how the endogenous
80 NAD+/NADH ratio of cancer cells is regulated to influence biosynthesis in different nutrient
81 depleted environments and its role in determining cancer cell proliferation when multiple oxidized
82 nutrients are limiting.

83 By culturing cancer cells in serine depleted conditions and examining the relationship
84 between the NAD+/NADH ratio and serine synthesis, we find that the NAD+/NADH ratio is
85 elevated in response to serine deprivation in some but not all cancer cells. The elevated
86 NAD+/NADH ratio is driven by increased mitochondrial respiration and promotes serine synthesis
87 to confer resistance to environmental serine depletion. A similar relationship between
88 mitochondrial respiration and the NAD+/NADH ratio was also observed in lipid depleted
89 environments, where higher mitochondrial respiration in some cells led to elevated NAD+/NADH
90 ratios and enhanced citrate synthesis. Lastly, we find that any perturbation that increases the
91 NAD+/NADH ratio, including lipid deprivation, could paradoxically improve the proliferation of cells
92 in serine depleted conditions. Together, these data reveal that the NAD+/NADH ratio is regulated
93 by mitochondrial respiration in response to environmental nutrients in a cancer cell-specific
94 manner and that this influences oxidative biosynthesis and proliferation. These data also provide
95 insight into how levels of multiple nutrients in tissue microenvironments may cooperate to enable
96 biomass synthesis and cell proliferation.

97

98 **Results**

99 **Modulating the cell NAD+/NADH ratio proportionally alters serine synthesis**

100 To begin investigating the processes that determine the cell NAD+/NADH ratio and
101 influence biomass synthesis, we examined the relationship between the NAD+/NADH ratio and
102 serine synthesis in serine-replete conditions (400 μM serine, the concentration of serine in DMEM)
103 and serine depleted conditions (DMEM media formulated without serine). Previous studies have
104 found that decreasing the cell NAD+/NADH ratio (more reduced) can suppress serine production
105 (Baksh, 2020; Bao, 2016; Broeks, 2023; Diehl, 2019). To confirm this, we varied the cell
106 NAD+/NADH ratio upon serine withdrawal and measured the serine synthesis rate of A549 non-
107 small cell lung cancer cells, which transcriptionally upregulate the serine synthesis enzyme
108 PHGDH (DeNicola, 2015). We increased the NAD+/NADH ratio by treating cells with the
109 exogenous electron acceptor alpha-ketobutyrate (AKB), which can be reduced to alpha-
110 hydroxybutyrate to regenerate NAD+ (Sullivan, 2015) (**Figure 1A**). We decreased the
111 NAD+/NADH ratio by treating cells with rotenone, an inhibitor of mitochondrial complex I, which
112 regenerates NAD+ in support of respiration. AKB and rotenone dose-dependently increased and
113 decreased the cell NAD+/NADH ratio, respectively (**Figure 1B**). To measure the serine synthesis
114 rate in cells, we performed kinetic isotope tracing using uniformly ^{13}C-labeled glucose (U-^{13}C-
115 glucose) and measured production of M+3 labeled serine (**Figure 1C**). Because intracellular
116 serine, including newly synthesized serine, rapidly exchanges with the extracellular environment
117 (Labuschagne, 2014), we collected both media and cells to help improve the detection of newly
118 synthesized serine produced from glucose. We find that increasing the cell NAD+/NADH ratio
119 with AKB led to proportionally higher serine synthesis rates whereas lowering the NAD+/NADH
120 ratio with rotenone led to proportionally lower serine synthesis rates (**Figure 1D**). This was not
121 explained by changes in PHGDH protein expression, as altering the NAD+/NADH ratio with AKB
122 or rotenone did not affect PHGDH protein levels despite modulating serine synthesis
123 (**Supplementary Figure 1A,B**). Additionally, neither rotenone treatment nor serine deprivation
124 had a large effect on cell viability (**Supplementary Figure 1C**). Of note, we find that serine
125 synthesis rate is positively correlated with the cell NAD+/NADH ratio (**Figure 1E**). Together, these

126 data demonstrate that modulating the NAD+/NADH ratio leads to proportional changes in serine
127 synthesis rates.
128
129 **Cancer cells with elevated NAD+/NADH ratios following serine withdrawal exhibit greater**
130 **serine synthesis**
131 Based on our finding that the NAD+/NADH ratio correlates with serine synthesis rate, we
132 wondered whether endogenous cell NAD+/NADH ratios, which can differ across cancer cells, are
133 predictive of proliferation rate following serine deprivation. To test this, we measured how
134 proliferation rate varied in a panel of cancer cells derived from various tissues-of-origin and with
135 different genetic driver mutations, and found a wide range of sensitivity to serine deprivation
136 (**Figure 2A**, **Supplementary Figure 2A, Supplementary Table 1**). Because PHGDH expression
137 is important for proliferation in serine depleted conditions (DeNicola, 2015; Locasale, 2011;
138 Maddocks, 2017; Possemato, 2011; Sullivan, 2019b), we first assessed the protein expression of
139 the serine synthesis enzymes PHGDH, PSAT1, and PSPH across the different cancer cells to
140 examine how well this explained environmental serine dependence. As expected, cells with low
141 serine synthesis enzyme protein levels (MCF7, MDA-MB-231) were most sensitive to serine
142 withdrawal while cells with higher serine synthesis enzyme protein levels were more resistant to
143 serine withdrawal (PHGDH-overexpressing MDA-MB-231, A375) (**Supplementary Figure 2A-C**).
144 However, for many cancer cells (Calu6, A549, 8988T, MIA PaCa-2, H1299, HCT116), serine
145 synthesis enzyme expression alone could not fully explain sensitivity to serine withdrawal
146 (**Supplementary Figure 2C**). For example, when comparing the non-small cell lung cancer cells
147 A549 and H1299, H1299 cells express less PHGDH protein and similar PSAT1 and PSPH protein
148 levels than A549 cells but are more resistant to serine deprivation **(Supplementary Figure 2B-**
149 **E)**. Consistent with lower PHGDH expression, H1299 cells express lower levels of NRF2, a
150 transcriptional regulator of serine biosynthesis enzymes (DeNicola, 2015). When examining the
151 cancer cells where serine synthesis enzyme expression could not fully explain the differences in

152 proliferation upon serine depletion, there was a surprising negative correlation between
153 proliferation and PHGDH protein expression, no relationship between proliferation and PSAT1
154 protein expression, and a positive correlation between proliferation and PSPH protein expression
155 (**Supplementary Figure 2F**). Given our finding that the NAD+/NADH ratio correlates with serine
156 synthesis rate, we hypothesized that differences in the NAD+/NADH ratio upon serine deprivation
157 could contribute to the variability in sensitivity to serine withdrawal across cells with similar serine
158 synthesis pathway protein levels. To test this, we measured the cell NAD+/NADH ratios in the
159 presence and absence of exogenous serine. Interestingly, we find that serine starvation elevated
160 the NAD+/NADH ratio in some cells, which we term “redox responder cells” and label in blue. In
161 contrast, we also find that certain cancer cells minimally change the NAD+/NADH ratio in
162 response to serine depletion, which we term “redox non-responder cells” and label in yellow
163 (**Figure 2B, Supplementary Figure 2G**). Of note, whether the NAD+/NADH ratio of a cell was
164 more or less oxidized in serine-replete conditions was not predictive of response to serine
165 withdrawal (**Supplementary Figure 2G)**. Strikingly, redox responder cells were more resistant to
166 serine depletion compared to redox non-responder cells (**Figure 2C**). The NAD+/NADH ratio was
167 also elevated in cancer cells with higher serine synthesis enzyme levels upon serine depletion
168 and were the most resistant to serine depletion (A375, PHGDH-overexpressing MDA-MB-231)
169 (**Supplementary Figure 2B,C,G**). To confirm that an elevated NAD+/NADH ratio in response to
170 serine depletion was associated with elevated serine synthesis, we compared how serine
171 synthesis rates changed following serine withdrawal in A549 and H1299 cells. We performed
172 focused comparisons between A549 and H1299 cells because they exhibit differences in
173 proliferation upon serine deprivation that are not explained by PHGDH protein expression,
174 demonstrate differing responses of the cell NAD+/NADH ratio upon serine deprivation, and have
175 similar basal proliferation rates. We find that after 24 hours in serine depleted conditions, H1299
176 cells demonstrated a higher rate of serine synthesis, a greater increase in serine synthesis, and
177 greater intracellular serine levels than A549 cells, consistent with the elevated NAD+/NADH ratio

178 in H1299 cells (**Figure 2D,E; Supplementary Figure 2H,I**). Importantly, we confirmed kinetic U-
179 ^{13}C-glucose tracing was performed at metabolic steady state by ensuring metabolite levels were
180 stable at each collected time point (**Supplementary Figure 2I**). Taken together, these data
181 suggest that in some cells, the cell NAD+/NADH ratio is responsive to serine availability. Moreover,
182 increases in the NAD+/NADH ratio correlate with increased serine synthesis and proliferation
183 rates in serine depleted conditions independent of PHGDH protein expression.
184

185 **Increased mitochondrial respiration is associated with an elevated NAD+/NADH ratio and**
186 **increased serine synthesis**

187 The finding that some cancer cells exhibit a more oxidized NAD+/NADH ratio upon serine
188 starvation is surprising, particularly when increased serine synthesis will result in a higher demand
189 for NAD+ to support increased flux through GAPDH and PHGDH (Diehl, 2019; Maddocks, 2017).
190 We hypothesized that a more oxidized NAD+/NADH ratio could support greater serine synthesis
191 and thus sought to identify the processes that increase the NAD+/NADH ratio in some but not all
192 cancer cells. Lactate production via lactate dehydrogenase (LDH) is a major NAD+ regenerating
193 process, particularly in cancer cells with high glucose fermentation (Fantin, 2006; Luengo, 2021;
194 Wang, 2022) (**Supplementary Figure 3A**); however, lactate secretion relative to glucose
195 consumption was not elevated following serine deprivation in any cells tested (**Supplementary**
196 **Figure 3B**). The NAD+ salvage pathway regenerates NAD+ from nicotinamide via nicotinamide
197 phosphoribosyl transferase (NAMPT) and nicotinamide mononucleotide adenylyltransferase
198 (NMNAT) and can be important for supporting PHGDH-driven serine synthesis (**Supplementary**
199 **Figure 3A**) (Murphy, 2018). While A549 cells were more sensitive to the NAMPT inhibitor FK866
200 in serine-replete conditions, there was no difference in the sensitivity of A549 and H1299 cells to
201 FK866 in serine depleted conditions (**Supplementary Figure 3C**). These data suggest that redox
202 responder and non-responder cells do not have differential dependency on the NAD+ salvage
203 pathway when cultured without serine. Moreover, supplementing redox non-responder A549 cells

204 with nicotinamide mononucleotide (NMN), a precursor to NAD+, did not improve proliferation in
205 serine depleted conditions (**Supplementary Figure 3D**). Mitochondrial respiration is another
206 major way cells regenerate NAD+ from NADH (Handy, 2012). Thus, we tested whether changes
207 in mitochondrial respiration, as measured by cellular oxygen consumption rate (OCR),
208 accompany the increase in the NAD+/NADH ratio following serine withdrawal. Indeed, cells that
209 increased their NAD+/NADH ratio following serine deprivation also exhibited increased OCR,
210 whereas cells with unaltered NAD+/NADH ratios following serine withdrawal did not (**Figure 3A,**
211 **Supplementary Figure 3E**). To test whether elevated oxygen consumption was related to serine
212 deprivation, we cultured H1299 and A549 cells in varying amounts of extracellular serine and
213 measured OCR. Oxygen consumption of A549 cells was not impacted by varying extracellular
214 serine levels, while oxygen consumption of H1299 cells increased as extracellular serine
215 decreased below 100 μM, the serine concentration where proliferation begins to be affected by
216 serine limitation (**Figure 3B, Supplementary Figure 3F**). The increase in OCR also
217 corresponded with the NAD+/NADH ratio at different serine levels in H1299 cells, while the
218 NAD+/NADH ratio in A549 cells was unchanged by extracellular serine availability (**Figure 3C,**
219 **D).** Consistently, the NAD+/NADH ratio of H1299 cells cultured in different concentrations of
220 serine positively correlated with serine synthesis, whereas A549 cells displayed minimal changes
221 in serine synthesis rate (**Figure 3E, F**). Notably, PHGDH protein levels remained constant as
222 extracellular serine levels were decreased in both A549 and H1299 cells (**Supplementary Figure**
223 **3G**). Together, these findings suggest that elevated NAD+/NADH ratios in response to decreasing
224 environmental serine are linked to elevated mitochondrial respiration in select cancer cells and
225 correlate with increased serine synthesis.
226
227 **Mitochondrial respiration governs the cell NAD+/NADH ratio and influences serine**
228 **synthesis rate**

229 To test whether increased mitochondrial respiration following serine depletion causes an
230 increase in the cell NAD+/NADH ratio, we treated redox non-responder cells with the proton
231 ionophore FCCP (trifluoromethoxy carbonylcyanide phenylhydrazone), which pharmacologically
232 increases mitochondrial oxygen consumption by uncoupling respiration from ATP synthesis
233 (McLaughlin, 1980; Terada, 1990). Increasing respiration with FCCP elevates mitochondrial
234 NAD+ regeneration and the cell NAD+/NADH ratio (Luengo, 2021) (**Figure 4A**). Indeed, FCCP
235 treatment improved proliferation of redox non-responder cells in serine depleted conditions
236 (**Figure 4B, Supplementary Figure 4A**). In contrast, FCCP did not improve the proliferation of
237 redox responder cells cultured without serine (**Figure 4C, Supplementary Figure 4B**).
238 Consistent with its impact on proliferation, FCCP treatment led to higher serine synthesis rates
239 only in redox non-responder A549 cells while having no impact on the serine synthesis rates of
240 redox responder H1299 cells (**Figure 4D,E, Supplementary Figure 5A-D**). As expected,
241 uncoupling mitochondrial respiration from ATP synthase with FCCP led to elevated oxygen
242 consumption in serine depleted A549 cells (**Figure 4F).** FCCP also increased oxygen
243 consumption in serine depleted H1299 cells (**Supplementary Figure 4C**). Interestingly, FCCP
244 raised the cell NAD+/NADH ratios of both A549 and H1299 cells following serine withdrawal
245 despite only improving serine synthesis and proliferation in A549 cells (**Figure 4G,**
246 **Supplementary Figure 4D**). The lack of impact on serine synthesis by FCCP in H1299 cells
247 suggests that NAD+ availability may not further constrain serine synthesis in cells that already
248 elevate mitochondrial respiration following environmental serine depletion. In this context, we
249 considered whether another constraint such as PHGDH protein expression was limiting serine
250 synthesis in redox responder cells treated with FCCP. Indeed, overexpressing PHGDH in serine
251 depleted redox responder H1299 and HCT116 cells fully restored proliferation to that observed in
252 serine-replete conditions (**Supplementary Figure 4E,G**). In contrast, proliferation of the redox
253 non-responder cells A549 and Calu6 following serine withdrawal had the greatest improvement
254 with simultaneous PHGDH overexpression and FCCP treatment (**Supplementary Figure 4F,G**).

255 This underscores that changes in both the cell NAD+/NADH ratio and relevant enzyme expression
256 impact serine synthesis in serine depleted environments. As an orthogonal approach to FCCP,
257 we constitutively expressed the NADH oxidase from *Lactobacillus brevis* (*Lb*NOX) in both the
258 cytoplasm and the mitochondria of A549 cells (**Supplementary Figure 6A**). We reasoned that if
259 expressing *Lb*NOX in either the cytoplasm or the mitochondrial were to raise the cell NAD+/NADH
260 ratio, proliferation of A549 cells upon serine depletion would be improved. To ensure *Lb*NOX
261 activity was present in cells, we treated cells with rotenone and measured proliferation. As
262 expected, we observed a proliferation improvement when *Lb*NOX was expressed in either the
263 cytoplasm or the mitochondria (**Supplementary Figure 6B**). However, A549 cyto*Lb*NOX and
264 mito*Lb*NOX cells did not exhibit an elevated cell NAD+/NADH ratio in either serine-replete or
265 serine depleted conditions (**Supplementary Figure 6C**), consistent with prior observations (Titov,
266 2016). There was also no change in proliferation upon serine withdrawal when *Lb*NOX was
267 expressed in the cytoplasm or mitochondria (**Supplementary Figure 6D**).

268 Because FCCP treatment led to a robust improvement in proliferation of redox non-
269 responder cells cultured without serine, we aimed to test whether FCCP improved serine
270 synthesis and proliferation of redox non-responder cells through oxidizing the NAD+/NADH ratio.
271 We treated cells with the mitochondrial complex I inhibitor rotenone in conjunction with FCCP.
272 Rotenone treatment ablated the ability of FCCP to improve both proliferation and serine synthesis
273 and blocked the ability of FCCP to increase the NAD+/NADH ratio (**Figure 4H-J, Supplementary**
274 **Figure 5E,F**). In contrast, treating cells with oligomycin, an ATP synthase inhibitor, did not affect
275 the ability of FCCP to improve proliferation (**Supplemental Figure 4H,I**). This supports the
276 conclusion that FCCP increases serine synthesis and proliferation in serine depleted
277 environments by increasing the NAD+/NADH ratio via mitochondrial complex I-mediated NAD+
278 regeneration. Moreover, FCCP treatment neither increased PHGDH protein expression nor
279 glucose consumption, indicating that improved proliferation and serine synthesis is not caused by
280 changes in enzyme expression or carbon availability for serine synthesis (**Supplementary Figure**

281 **4J,K**). Together, these data argue that mitochondrial respiration, either endogenously increased
282 in response to serine deprivation, or as a result of FCCP treatment, can govern the cell
283 NAD+/NADH ratio and directly influence the serine synthesis rate in response to serine withdrawal.
284

285 **The malate aspartate shuttle enzymes MDH1 and GOT2 support elevated mitochondrial**
286 **respiration in redox responder H1299 cells in serine-depleted environments**

287 The malate aspartate shuttle (MAS) transports reducing equivalents between the
288 cytoplasm and the mitochondria and can be important for de novo serine synthesis (Broeks, 2023).
289 Thus, we hypothesized that in serine-deplete H1299 cells, the MAS allows increases in
290 mitochondrial respiration to support cytosolic serine synthesis. To test this, we used
291 CRISPR/Cas9 in H1299 cells to generate isogenic cell lines where either GOT1, MDH1, or GOT2
292 was deleted (**Supplementary Figure 7A**). Using these knock-out cell lines, we measured
293 proliferation in serine depleted conditions and found that MDH1 and GOT2 knock-out cell lines
294 were more sensitive to serine deprivation compared to non-targeting controls (NTC)
295 (**Supplementary Figure 7B**). We then measured the cell NAD+/NADH ratio in knock-out cells
296 cultured without serine and observed that unlike H1299 NTC and GOT1 KO cells, H1299 MDH1
297 and GOT2 KO cells did not exhibit elevated NAD+/NADH ratios upon serine depletion
298 (**Supplementary Figure 7C**). Consistently, unlike H1299 NTC cells, H1299 MDH1 and GOT2 KO
299 cells did not demonstrate elevated mitochondrial respiration upon serine depletion
300 (**Supplementary Figure 7D**). This corresponded with H1299 MDH1 and GOT2 KO cells having
301 blunted serine synthesis rates compared to H1299 NTC cells (**Supplementary Figure 7E**).
302 Together, this suggests that MDH1 and GOT2 activity support the process by which mitochondrial
303 NAD+ regeneration is transmitted to the cytoplasm to support serine synthesis.
304

305 **The NAD+/NADH ratio influences oxidative citrate synthesis in either serine- or lipid-**
306 **depleted environments**

307 Oxidative biosynthetic reactions other than serine synthesis can also be constrained by
308 the NAD+/NADH ratio. For example, cancer cells deprived of environmental lipids increase
309 oxidative citrate production, and we have previously found that citrate synthesis, either through
310 glucose oxidation or glutamine oxidation, is limited by NAD+ availability (Li, 2022) (**Figure 5A,**
311 **Supplementary Figure 8A**). Thus, we sought to uncover whether the increase in the cell
312 NAD+/NADH ratio by mitochondrial respiration in response to serine withdrawal specifically
313 supports greater serine synthesis or also leads to greater oxidative citrate production. To answer
314 this question, we first assessed labeled citrate production using kinetic U-^{13}C-glucose tracing in
315 cells that showed increased NAD+/NADH ratios following serine deprivation. We found that the
316 redox responder cells largely showed elevated M+2 citrate production despite no change in
317 environmental lipid availability (**Figure 5B; Supplementary Figure 8B-E**). In contrast, cells with
318 unaltered NAD+/NADH ratios upon serine depletion did not exhibit higher M+2 citrate production
319 **(Figure 5B; Supplementary Figure 8B, F-H)**. Consistently, redox responder H1299 cells, but
320 not redox non-responder A549 cells, displayed evidence of elevated citrate production from
321 glutamine either through oxidative decarboxylation or reductive carboxylation, both of which
322 require oxidation reactions that can be limited by electron acceptor availability (Hosios and Vander
323 Heiden, 2018; Li, 2022) (**Supplementary Figure 8I, J**). To confirm that elevated M+2 citrate
324 synthesis was driven by an increase in the NAD+/NADH ratio, we treated A549 cells depleted of
325 serine with FCCP and examined glucose-derived citrate synthesis. Indeed, FCCP treatment led
326 to a four-fold increase in M+2 citrate from U-^{13}C-glucose in A549 cells depleted of serine whereas
327 M+2 citrate synthesis was less affected by FCCP in H1299 cells (**Figure 5C**). The elevated M+2
328 citrate production in FCCP-treated A549 cells was dependent on mitochondrial complex I, as
329 rotenone prevented the elevated citrate production associated with FCCP treatment
330 (**Supplementary Figure 9A-C**). To confirm that higher M+2 citrate production following FCCP
331 treatment was related to the NAD+/NADH ratio independent of serine deprivation, we treated
332 A549 cells with increasing doses of AKB and FCCP in serine-replete conditions and find that

333 increasing the NAD+/NADH ratio with either AKB or FCCP led to elevated M+2 citrate synthesis
334 (**Figure 5D**). This argues that changes to the NAD+/NADH ratio regardless of the nutrient
335 environment can impact citrate synthesis.

336 We next asked whether increasing mitochondrial respiration in response to low
337 extracellular serine was specific to serine deprivation or represented a general response to any
338 nutrient deprivation that increased NAD+ demand, such as lipid deprivation (Li, 2022). To examine
339 this, we depleted A549 and H1299 cells of extracellular lipids by culturing cells in media with lipid-
340 depleted serum (Hosios, 2018) and compared oxygen consumption rates to those of cells cultured
341 in media with lipid-containing serum. Surprisingly, we find that A549 cells, which do not increase
342 mitochondrial respiration in response to serine depletion, showed a trend towards a mildly
343 elevated oxygen consumption rate upon lipid depletion (**Figures 5E**). On the other hand, H1299
344 cells do not increase oxygen consumption in lipid depleted conditions (**Figure 5E**). We next
345 measured the NAD+/NADH ratio of A549 and H1299 cells depleted of environmental lipids.
346 Consistent with the changes in oxygen consumption, A549 cells displayed an increased
347 NAD+/NADH ratio while H1299 cells did not alter the NAD+/NADH ratio upon lipid deprivation
348 (**Figure 5F**). Interestingly, both serine and citrate produced via glucose oxidation was elevated in
349 lipid depleted A549 cells in comparison to H1299 cells, which exhibited unchanged serine
350 synthesis in response to environmental lipid depletion (**Figure 5G-H, Supplementary Figure 10**).
351 These findings suggest that the NAD+/NADH ratio can be a determinant of both oxidative citrate
352 and serine synthesis, regardless of environmental demand for the nutrient. Additionally, the
353 different metabolic responses to lipid and serine deprivation between cancer cell types suggests
354 that different nutrient environments impact mitochondrial respiration through distinct processes to
355 influence the NAD+/NADH ratio.

356

357 **Lipid depletion can enhance proliferation in serine deprived conditions**

358 Our finding that both serine and oxidative citrate synthesis can be impacted by levels of a
359 different nutrient than that produced by each pathway raised the possibility that the NAD+/NADH
360 ratio coordinates biomass synthesis in response to the availability of multiple oxidized nutrients.
361 Specifically, we hypothesized that changes to the NAD+/NADH ratio caused by one oxidized
362 nutrient depletion could influence the synthesis of, and in turn the dependency on, another
363 oxidized nutrient for proliferation. To begin testing this, we first examined how mitochondrial
364 respiration and the NAD+/NADH ratio were impacted by dual lipid and serine depletion compared
365 to single nutrient depletions in both A549 and H1299 cells. We find that dual depletion of serine
366 and lipids in A549 cells led to elevated oxygen consumption that is higher than that observed with
367 serine depletion alone **(Figure 6A)**. Similarly, dual depletion of serine and lipids in H1299 cells
368 led to elevated oxygen consumption compared to that observed with lipid depletion alone **(Figure**
369 **6A)**. The resulting oxygen consumption rate corresponded with the cell NAD+/NADH ratio in each
370 condition, which was collectively higher upon dual serine and lipid starvation than either serine
371 depletion in A549 cells or lipid depletion in H1299 cells (**Figure 6B**). We then measured the serine
372 and citrate synthesis rates of cells depleted of both extracellular serine and lipids via kinetic U-
373 ^{13}C-glucose tracing. Consistent with elevation of the NAD+/NADH ratio after lipid deprivation,
374 A549 cells depleted of both environmental serine and lipids trended towards elevated serine
375 synthesis rates when compared to serine deprivation alone, though was not statistically significant
376 **(Figure 6C).** Moreover, lipid depletion appeared to lead to a greater fraction of total serine derived
377 from glucose in serine depleted A549 cells **(Supplementary Figure 11A)**. In contrast, lipid
378 starvation did not alter serine synthesis in serine deprived H1299 cells (**Figure 6D,**
379 **Supplementary Figure 11A,B**). Interestingly, in both A549 and H1299 cells, dual serine and lipid
380 deprivation led to a trend toward increased citrate production compared to lipid deprivation alone
381 despite only H1299 cells exhibiting a more oxidized NAD+/NADH upon serine depletion (**Figure**
382 **6E,F; Supplementary Figure 11C,D)**. This underscores the multifactorial regulation of glucose
383 oxidation to citrate (Holness, 2003; Novelli, 1950; Patel, 2006; Srere, 1974). We next asked how

384 cancer cell proliferation was impacted by dual serine and lipid depletion compared to single
385 nutrient depletions. Strikingly, proliferation of serine depleted A549 cells was improved with
386 depletion of extracellular lipids (**Figure 6G**), consistent with the elevation in mitochondrial
387 respiration, NAD+/NADH ratio, and a trend towards greater serine synthesis in A549 cells upon
388 dual serine and lipid depletion. Unlike serine depletion, lipid depletion does not cause a major
389 proliferation defect in either A549 or H1299 cells, and dual serine and lipid deprivation did not
390 greatly alter the proliferation of H1299 cells compared to serine depletion alone (**Figure 6H**). This
391 is consistent with lipid deprivation causing no major changes in oxygen consumption,
392 NAD+/NADH ratio, and serine synthesis in H1299 cells. These data argue that the cell
393 NAD+/NADH ratio is modulated in response to multiple nutrient availabilities in a cancer cell-
394 specific fashion. The changes in NAD+/NADH ratio in turn may influence the capacity for serine
395 and citrate synthesis, impacting the proliferation rate of cancer cells in nutrient environments with
396 differing demands for oxidative biomass synthesis. Taken together, we propose a model where
397 environmental nutrient availability can impact mitochondrial respiration based on the specific
398 cancer. Because mitochondrial respiration is a major pathway that regenerates NAD^+, changes
399 to mitochondrial respiration can alter the cell NAD+/NADH ratio, influencing the activity of major
400 NAD^+-requiring metabolic reactions such as serine synthesis and citrate synthesis that can be
401 important for proliferation. We further propose that changes to the cell NAD+/NADH ratio can
402 impact all oxidative biosynthetic reactions if the enzyme machinery is present, but that specificity
403 for how the cell NAD+/NADH ratio changes is dependent on both cell-intrinsic factors and cell-
404 extrinsic factors (**Figure 7**).
405
406 **Discussion**
407 Proliferating cancer cells must acquire sufficient biomass and rely on contributions from
408 both environmental nutrients and de novo synthesis pathways, but what determines which cells
409 can adapt to different nutrient environments that impose constraints on salvage and synthesis is

410 not known. This study highlights that differential cell responses to changes in the NAD+/NADH
411 ratio enable biomass synthesis and determine whether cells can adapt to proliferate in different
412 nutrient conditions. Importantly, this provides one explanation for why single nutrient levels in
413 tissues may not predict the ability of auxotrophy for that nutrient to determine cancer proliferation
414 in a tissue (Abbott, 2026). It also suggests why cancer proliferation in different nutrient
415 environments is controlled by a complex relationship between cell-intrinsic and cell-extrinsic
416 factors. These factors may be coordinated in part through processes that set the NAD+/NADH
417 ratio in cells.

418 Most prior work to determine what shapes the metabolic dependencies of cell proliferation
419 has focused on factors that govern biosynthetic enzyme expression and activity. For example,
420 genomic and transcriptional analyses of cancer discovered that increased PHGDH expression
421 promotes tumor growth (DeNicola, 2015; Locasale, 2011; Newman, 2017; Possemato, 2011) and
422 provides a proliferative advantage in serine depleted tumor microenvironments (Ngo, 2020;
423 Sullivan, 2019b). Our findings show that enzyme expression alone cannot fully explain nutrient
424 dependencies, as PHGDH expression can be discordant with sensitivity to serine depletion.
425 Rather both the NAD+/NADH ratio and enzyme expression play integral roles in determining
426 cancer proliferation in specific nutrient environments. These data are consistent with biosynthetic
427 gene expression and single nutrient levels being unable to predict the tumor tissue environments
428 where cancer cells can form metastases (Abbott, 2026).

429 Extensive work has highlighted the importance of cell NAD+/NADH ratio in influencing
430 oxidized biomass production, nutrient utilization, and nutrient dependencies (Baksh, 2020; Bao,
431 2016; Birsoy, 2015; Broeks, 2023; Christensen, 2014; Diehl, 2019; Garcia-Bermudez, 2018;
432 Gibson, 1976; Krall, 2021; Li, 2022; Sullivan, 2015; Wu, 2024). Yet, the processes that govern
433 the endogenous NAD+/NADH ratio upon shifts in nutrient availability have been largely
434 uncharacterized. We find that regulation of mitochondrial respiration is a major mechanism that
435 dictates the NAD+/NADH ratio in response to environmental nutrient fluctuations. The

436 mitochondrial respiration response to withdrawal of specific nutrients appears to vary across
437 different cancer cells. Some cancer cells increased mitochondrial respiration to serine depletion,
438 while others had minimal responses. We found that in serine redox responder cancer cells, the
439 malate aspartate shuttle (MAS) enzymes MDH1 and GOT2 were required for the elevation in
440 mitochondrial respiration and the NAD+/NADH ratio in response to serine depletion. Thus,
441 differences in the activity of MAS, which can vary greatly across cancer cells (Wang, 2022), may
442 influence the capacity for cancer cells to increase mitochondrial respiration and NAD+
443 regeneration to support oxidative biosynthetic pathways. Interestingly, serine is an allosteric
444 activator of the glycolytic enzyme pyruvate kinase, which converts phosphoenolpyruvate to
445 pyruvate and generates ATP (Chaneton, 2012). Thus, decreased environment serine availability
446 in addition to differences in pyruvate kinase activity may yield lower glycolytic ATP, resulting in
447 greater mitochondrial respiration in serine redox responder cancer cells. Additionally, it has been
448 recently shown that differences in mtDNA in non-small cell lung cancer cells can lead to defective
449 mitochondrial respiration and imbalanced NAD+/NADH ratios, suppressing serine synthesis and
450 tumor growth (Lopes, 2025). These findings suggest some reasons why respiration may be
451 differentially responsive to serine withdrawal. However, lipid depletion yielded mitochondrial
452 respiration changes in cancer cells that did not respond to serine withdrawal, arguing against
453 respiration defects explaining non-response. No clear common genetic factor or tissue-of-origin
454 was found to align with those cells that do or do not have mitochondrial and redox responses to
455 serine and/or lipid depletion. Further work is needed to understand the mechanisms that enable
456 increased mitochondrial respiration in response to deprivation of different nutrients. One
457 possibility is that differences in ATP consumption following nutrient deprivation contribute to the
458 response. Stimulating ATP consumption can increase mitochondrial respiration and the
459 NAD+/NADH ratio (Bertholet, 2019; Buttgereit, 1995; Fisher-Wellman, 2012; Luengo, 2021;
460 Nobes, 1989; Vander Heiden, 1999). ATP synthase activity can restrain complex I activity to
461 different extents across cancers, modulating the endogenous NAD+/NADH ratio and sensitivity

462 to serine or lipid depletion. While the regulation of complex I, ATP synthesis, and mitochondrial
463 coupling efficiency is complicated and incompletely understood (Alavian, 2014; Gao, 2018;
464 Lapuente-Brun, 2013; Luengo, 2021; Qiu, 2014; Wang, 2022; Yao, 2019; Zhao, 2019), our
465 findings suggest an important connection between the regulation of mitochondrial bioenergetics
466 and specific metabolic vulnerabilities of cancer growth, underscoring an important relationship
467 between environmental nutrient levels and mitochondrial respiration to influence the cell
468 NAD+/NADH ratio.

469 Efforts to understand the processes that shape cancer cell metabolic dependencies have
470 largely focused on how cancer cells respond to single nutrient changes. However, findings from
471 dual serine and lipid depletion experiments suggest that single nutrient availabilities will be unable
472 to explain cancer metabolic dependencies in some contexts. For example, depleting A549 cells
473 of both extracellular serine and lipids paradoxically improved proliferation relative to serine
474 deprivation alone, consistent with an elevated NAD+/NADH ratio in response to lipid deprivation
475 that can support greater serine synthesis. This suggests that the NAD+/NADH ratio can serve as
476 a metabolic regulatory node that orchestrates biomass synthesis and integrates changes to
477 multiple oxidized biomass components in the environment, providing a framework for
478 understanding why cancer nutrient dependencies vary across tissue microenvironments (Abbott,
479 2026). Because oxidizing the cell redox state can increase flux through multiple pathways, the
480 impact of cell redox state on biosynthesis may also explain why some cells lose enzyme
481 expression in pathways like serine synthesis, as this could redirect limited resources toward
482 biomass components that can otherwise be scavenged from the environment (Delage, 2010;
483 Pavlova, 2017; Rabinovich, 2015). Better understanding the mechanisms cells use to alter
484 respiration and adjust the NAD+/NADH ratio in response to available nutrients could inform the
485 complex interplay between cell-intrinsic and cell-extrinsic factors that determine cancer metabolic
486 dependencies. This is particularly important to consider when targeting metabolism for cancer
487 treatment. Many newer therapies targeting metabolism have not been successful in part because

488 of metabolic plasticity to nutrient shifts (Amoedo, 2017; Fendt, 2020; Xiao, 2023). Co-targeting
489 mitochondrial function limits metabolic adaptations and may also help predict the tissue nutrient
490 conditions that result in pathway dependencies for specific cancers. Thus, better understanding
491 how the cell NAD+/NADH ratio responds to nutrient levels in different cancers could improve
492 selection of patients for cancer therapies that impact metabolism.
493

494 **Material and Methods**

495 **Cell Culture Experiments**

496 Cell lines were maintained in Dulbecco's Modified Eagle's Medium (DMEM) without sodium
497 pyruvate (Corning 50-013-PC) supplemented with sodium bicarbonate (Sigma S6014) and 10%
498 heat-inactivated Fetal Bovine Serum (FBS). All cells were cultured at 37°C with 5% CO_2, tested
499 for mycoplasma contamination regularly, and confirmed negative before experimentation. Cell
500 line information is listed in Supplementary Table 1.
501

502 **Proliferation Assays**

503 Cells were plated in six-well plates in 2 ml of DMEM with 10% heat-inactivated FBS at an initial
504 seeding density of 40,000 cells. Cells were permitted to settle overnight and then quantified using
505 a sulforhodamine B (SRB) (Sigma Aldrich 230162) colorimetric assay to measure the starting cell
506 absorbance at the start of the experiment as previously described (Vichai, 2006). For treatment
507 conditions, cells were washed three times with 1 ml of 1X PBS, and 2 ml of treatment media were
508 added to each well. All treatment media was made with 10% dialyzed FBS. Serine-free medium
509 was made by adding a mix of amino acids (Sigma Aldrich) at DMEM concentrations lacking serine
510 and glycine to DMEM with low glucose, without sodium pyruvate, and amino acids (US Biological
511 D9800-13-50L). Glucose and glycine were supplemented for a final concentration for 25 mM and
512 0.4 mM, respectively. Three days after the initial treatment, cells were quantified using SRB assay.

513 All SRB measurements are normalized to a blank to correct for background signal. Proliferation
514 rates were calculated with the following formula:

515 $$\text{Doublings per day} = \frac{\log_2(\text{final SRB absorbance} / \text{SRB absorbance day 0})}{(\text{total \# of treatment days})}$$

516

517

518 **Cell Number and Viability Measurements**

519 Cells were seeded at an initial density of 2,000 cells per well in a 96-well plate in 200 µl of
520 treatment media. After allowing cells to settle for 1-2 hours, cell number was monitored over time
521 using imaging with the Incucyte Live-Cell Analysis System (Sartorius). Doublings per day were
522 calculated between hour 0 of monitoring and hour 72 of monitoring using the following formula:

523 $$\text{Doublings per day} = \frac{\log_2(\text{cell number at hour 72} / \text{cell number at hour 0})}{(\text{3 days of treatment})}$$

524

525 For viability, cells were seeded at an initial density of 2,000 cells per well in a 96-well plate in 200
526 µl of treatment media with 20 nM Sytox Green (Invitrogen S7020). After 72 hours, the number of
527 live and dead cells present was monitored using imaging with the Incucyte Live-Cell Analysis
528 System (Sartorius).

529

530 **NAD+/NADH Measurements**

531 NAD+/NADH measurements were performed using the NAD/NADH-Glo Assay (Promega G9072)
532 with a modified version of manufacturer instructions as previously reported (Sullivan, 2015). Cells
533 were plated at an initial seeding density of 20,000 cells (A549, H1299, HCT116) or 40,000 cells
534 (Calu6, MDA-MB-231). Cells were permitted to settle overnight. The next day, cells were washed
535 once with 1X PBS and then incubated with 2 ml of treatment media for the indicated times prior
536 to preparation of cell extracts. For extraction, cells were washed once in ice cold 1X PBS and
537 extracted in 100 µl ice-cold 1% dodecyltrimethylammonium bromide (DTAB) in 0.2N NaOH diluted
538 1:1 with 1X PBS. Each sample was flash-frozen in liquid nitrogen and immediately stored at -

539 80°C. To measure NADH, 10 µl of sample was moved to PCR tubes, diluted with 10 µl of DTAB,
540 and incubated at 75 °C for 30 min, where basic conditions selectively degrade NAD+. To measure
541 NAD+, 10 µl of the samples was moved to PCR tubes containing 30 µl DTAB and 20 µl 0.4 N HCl
542 and incubated at 60°C for 15 min, where acidic conditions selectively degrade NADH. Samples
543 were then allowed to equilibrate to room temperature and quenched by neutralizing with 20 µl
544 0.25 M Tris in 0.2 N HCl (for NADH) or 20 µl 0.5 M Tris base (for NAD+). Manufacturer instructions
545 were followed thereafter to measure NAD+/NADH using a luminometer (Tecan Infinite M200Pro).
546 A standard curve with representative samples was done with each assay to confirm that NAD+
547 and NADH measurements were in the linear range of detection.

548 **Glucose Consumption and Lactate Secretion Measurements**

549 Cells were plated at a density of 40,000 cells per well in a six well plate. The next day, cells were
550 washed three times with 1X PBS before 2 ml of treatment media were added to each well. In
551 parallel, 2 ml of treatment media were added to plates without cells. An initial cell number before
552 beginning treatment was quantified via Cellometer (Nexcelom Bioscience). 72 hours later, media
553 was collected from exponentially proliferating cells with a parallel collection of media from wells
554 without cells, which we used to measure initial media concentrations to take into consideration
555 evaporative changes. Cell number was quantified via Cellometer along with the volume of media
556 on cells to consider evaporative changes to metabolite concentrations that may have occurred
557 over 72 hours in culture. Glucose concentrations from media samples were measured on a YSI-
558 2900 Biochemistry Analyzer (Yellow Spring Instruments). Every assay included a glucose (Sigma
559 Aldrich G8270) standard curve (0, 2.5, 5, 10, 20, and 40 mM glucose) and lactate (Sigma Aldrich
560 71716) standard curve (0, 1.25, 2.5, 5, 10, and 20 mM sodium lactate), made in both control and
561 treatment media. To calculate consumption rate per cell for a given nutrient, fmol of glucose or
562 lactate over time were plotted relative to the area under the curve (fmol / cells · time) of an

563 exponential function fit to the number of cells at the start of the assay and after 72 hours of
564 treatment, as previously described (Hosios, 2016).
565
566 **Oxygen Consumption Measurements**
567 An Agilent Seahorse Bioscience Extracellular Flux Analyzer (XFe96) was used to measure
568 oxygen consumption rates (OCR). Cells were plated at 20,000 – 40,000 cells per well in a
569 Seahorse Bioscience 96-well plate in 80 µl of DMEM without pyruvate supplemented with 10%
570 heat-inactivated FBS. Cells were not plated on the perimeter of the plate to avoid edge effect.
571 The following day, cells were washed twice with 180 µl of treatment media supplemented with 10%
572 dialyzed FBS before incubating cells with 180 µl of treatment media for the indicated time prior to
573 OCR data acquisition. For 24 hour treatment periods, treatment media was replaced with 180 µl
574 of fresh treatment media two hours before OCR data acquisition. The day before OCR data
575 acquisition, the XFe96 cartridge was hydrated by submerging the sensor cartridge in 200 µl of
576 sterile water per well of the utility plate. Parafilm was wrapped around the perimeter of the
577 cartridge to avoid evaporation. The XFe96 cartridge was then incubated in a 37°C non-CO_2
578 incubator overnight. The next day, at least two hours before data acquisition, the water in the
579 utility plate was replaced with 200 µl of the Agilent XF Calibrant per well and the sensory cartridge
580 was submerged and returned to the 37°C non-CO_2 incubator until OCR was ready to be measured.
581 After OCR data acquisition, six to eight wells per treatment condition were collected for cell
582 number quantification (Cellometer) to normalize OCR values. Basal OCR was calculated by
583 subtracting residual OCR, the OCR remaining following the addition of rotenone and antimycin A
584 for a final concentration of 2 µM.
585
586 **Kinetic U-^{13}C-Glucose Isotope Tracing Experiments**
587 Cells were seeded at 150,000 cells per well in a six-well plate in 2ml of DMEM without sodium
588 pyruvate supplemented with 10% heat-inactivated FBS. The following day, cells were washed

589 once with 1ml of 1X PBS and then incubated in 2ml of treatment media supplemented with 10%
590 dialyzed FBS for the indicated treatment time and when metabolic steady state is reached. Two
591 hours before the start of the kinetic isotope tracing, media on cells was exchanged with fresh
592 treatment media with 10mM unlabeled glucose. To measure serine labeling over time in serine
593 depleted conditions, cells and media were extracted together. Before the initiation of the kinetic
594 U-^{13}C-glucose isotope tracing, serine-deplete cells were washed three times with 1X PBS and
595 then cultured with 400 µl of tracing medium containing 10 mM of U-^{13}C-glucose (Cambridge
596 Isotope Laboratories, CLM-481-0) for the rapid time points. Tracing media was equivalent to
597 treatment media except with 10 mM of U-^{13}C- glucose. Following incubation, 1.6ml of extraction
598 buffer containing ice cold 100% HPLC-grade methanol (Sigma Aldrich, 646377) with norvaline
599 (Sigma, N7627) was added onto cells with tracing media for a final sample volume of 2 ml (80%
600 extraction buffer and 20% tracing media) and a final concentration of 1 µg per 400 µl norvaline.
601 1.6 ml of the lysate was placed into a fresh Eppendorf tube, vortexed at 4°C at maximum speed
602 for ten minutes, and then spun down at 4°C at maximum speed for thirty minutes. The supernatant
603 was collected and dried under nitrogen gas to prepare for metabolic analysis. To measure serine
604 and citrate production in serine replete conditions, only intracellular metabolites were quantified.
605 Before the initiation of kinetic U-^{13}C-glucose isotope tracing, serine-replete cells were washed
606 three times with 1X PBS and then cultured with 1 ml of tracing medium containing 10 mM of U-
607 ^{13}C-glucose (Cambridge Isotope Laboratories, CLM-481-0) for the rapid time points. Tracing
608 media was equivalent to treatment media except with 10 mM of U-^{13}C- glucose. Following
609 incubation, cells were rapidly washed twice with ice cold blood bank saline. To extract, 500 µl of
610 extraction buffer containing 80% ice cold HPLC-grade methanol and 20% LC-grade water spiked
611 with 1 µg per 400 µl norvaline were added onto cells. Cells were then lysed as previously
612 described above.
613
614 **Gas Chromatography-Mass Spectrometry (GC-MS) Polar Metabolite Measurements**

615 Dried samples were derivatized by adding 16 µl of methoxamine reagent (Thermo Fisher, TS-
616 45950) and incubated for an hour at 37°C followed by the addition of 20 µl of *N-tert-*
617 butyldimethylsilyl-*N*-methyltrifluoroacetamide with 1% *tert*-butyldimethylchlorosilane (Sigma
618 375934). Samples were then incubated for two hours at 60°C. Afterwards, samples were
619 centrifuged at maximum speed for ten minutes, and 20 µl of supernatant was used for analysis.
620 Following derivatization, samples were analyzed using a DB-35MS column (30 m × 0.25 mm
621 i.d. × 0.25 µm, Agilent J&W Scientific) in an Agilent 7890 gas chromatograph coupled to an Agilent
622 5975C mass spectrometer (GC–MS). All ion counts were normalized to internal standard
623 norvaline and cell number measured via Cellometer.
624
625 **Immunoblotting**
626 Cells were washed with ice cold 1X PBS and lysed in cold RIPA buffer containing Halt Protease
627 and Phosphatase Inhibitor Cocktail (Thermo Scientific 78442). Lysates were clarified by rocking
628 samples for thirty minutes at 4°C and then spun at maximum speed for ten minutes for collection
629 of supernatants. Protein concentration was calculating using the BCA Protein Assay (Pierce,
630 23225) with BSA as a standard. Lysates were resolved by SDS-PAGE using NuPAGE 4-12% Bis-
631 Tris Protein Gels (Thermo Fisher Scientific) and run at 100V. Proteins were transferred onto
632 nitrocellulose membranes via wet transfer at 100V. Membranes were blocked in 5% BSA in 1x
633 TBST before incubating membranes with primary antibodies at 4°C overnight. The next day,
634 membranes were washed three times with 1x TBST at room temperature and then incubated in
635 secondary antibodies for one hour at room temperature. The primary antibodies used were
636 PHGDH (Sigma Aldrich, HPA021241 [1:1000]), PSAT1 (Abcam, ab96136 [1:1000]), PSPH
637 (Abcam, ab96414 [1:1000]), HSP90 (Cell Signaling Technology, 4874 [1:1000]), Vinculin (E1E9V)
638 XP® (Cell Signaling Technology, 13901 [1:1000]), GOT1 (Cell Signaling Technology, 34423S
639 [1:1000], MDH1 (MDHC H-6, Santa Cruz Biotechnology, sc-166879 [1:1000]), GOT2 (Cell
640 Signaling Technology, 71692S [1:1000]), FLAG (Cell Signaling Technology, 14793 [1:1000]). The

641 secondary antibodies used were anti-rabbit IgG horseradish peroxidase-linked antibody (1:4000
642 dilution; Cell Signaling Technologies, 7074S) or anti-mouse IgG horseradish peroxidase-linked
643 antibody (1:4000, 7076S). Protein expression was quantified by using ImageJ analysis.
644
645 **Genetic Manipulation of Enzyme Expression in Cells**
646 Cell lines overexpressing either EGFP or human PHGDH were generated via lentiviral infection.
647 pLJM1-EGFP was obtained from Addgene (Addgene 19319). pLJM1-PHGDH was constructed
648 using pLJM1-Empty (Addgene 91980) as a backbone. pLJM1-Empty was digested using NheI
649 and EcoRI and gel purified. Human PHGDH cDNA was amplified from pLHCX-PHGDH (PMID:
650 31598584) with the following oligonucleotide primers, where the capitalized sequence denotes
651 PHGDH homology:
652 PHGDH F: agtgaaccgtcagatccggctagcgccaccATGGCTTTTGCAAATCTGCG
653 PHGDH R: tactgccatttgtctcgaggtcgagaattcTTAGAAGTGGAACTGGAAGGCT
654 PHGDH insert was gradient PCR amplified using Phusion High-Fidelity DNA polymerase (NEB
655 M0530) from 60 to 70°C and gel purified. Digested pLJM1-Empty and amplified PHGDH insert
656 were assembled via Gibson Assembly, and the resulting plasmid was transformed, and
657 validated by Sanger sequencing. Lentiviral production was done by transfecting constructs into
658 LentiX293T cells with Mirus Transit293T (Mirus Bio MIR2700) following manufacturer's protocol.
659 Briefly, 800,000 cells were plated per well in a 6 well plate in DMEM media with 10% heat-
660 inactivated FBS. The next day, cells were transfected with 1.6 µg vector (either pLJM1-EGFP or
661 pLJM1-PHGDH), 800 ng of pMDLg (Addgene 12251) packaging plasmid, 400 ng of pMD2.G
662 (Addgene 12259) envelope plasmid, and 400 ng of pRSV-REV (Addgene 12253) in OptiMEM
663 (Thermo Fisher Scientific 31985070). DNA transfection mix was incubated with cells for 48
664 hours before harvesting virus and filtering through a 0.45 µm polyethersulfone membrane. Sub-
665 confluent cells were infected with 1 ml of virus-containing media in each well of a 6 well plate
666 with polybrene (8 µg/ml, EMD Millipore TR-1003-G). 24 hours after infection, selection with 1

667 μg/mL puromycin (Sigma Aldrich P7255) began. All experiments with generated cell lines
668 expressing PHGDH were conducted on polyclonal cell populations.
669 cyto*Lb*NOX-FLAG cDNA and mito*Lb*NOX-FLAG cDNA were PCR amplified from
670 pUC57-*Lb*NOX or pUC57-mito*Lb*NOX, respectively. pUC57-*Lb*NOX (Addgene 75285) and
671 pUC57-mito*Lb*NOX (Addgene 74448) were a gift from Vamsi Mootha. The PCR products were
672 subsequently cloned into pLJM1 using Gibson Assembly (NEB E2611S). pLJM1-EGFP was a
673 gift from David Sabatini (Addgene 19319). Cells were then transduced with lentivirus containing
674 pLJM1-*Lb*NOX-FLAG, pLJM1-mito*Lb*NOX-FLAG, or pLJM1-EGFP. The infected cells were
675 selected in 1 μg/mL puromycin (Sigma Aldrich P7255). All experiments with generated cell lines
676 involving *Lb*NOX were conducted on a polyclonal cell population.
677 GOT1, GOT2, and MDH1 Knockout H1299 cells were generated by using lentiCRISPRv2
678 (Addgene 52961). LentiCRISPRv2 was a gift from Feng Zhang. Guide RNAs (gRNAs) for each
679 gene of interest were designed by CRISPick
680 (https://portals.broadinstitute.org/gppx/crispick/public) and cloned into lentiCRISPRv2. The
681 guide sequences used are as follows:
682 NTC: GTGTAGTTCGACCATTCGTG
683 GOT1: GGAGGTGTGCAATCTTTGGG
684 GOT2: CGGACGCGGGTCCACTCCCG
685 MDH1: CGTCCAGGACACCCATCATG
686 Cell lines were generated by transducing cells with viral particles containing lentiCRISPRv2
687 followed by selection with 1 μg/mL puromycin (Sigma Aldrich P7255). Single cells were plated
688 into individual wells of 96 well plates in RPMI medium to obtain single clone knock out cells.
689 Following expansion, immunoblotting was used to confirmed complete knockout.
690
691 **Statistics and Reproducibility**

692 All statistical tests using experimental data were performed with Prism 10 software. No statistical
693 method was used to predetermine sample sizes. Samples sizes were chosen based on pilot
694 experiments using three or more technical replicates. The experiments were not randomized and
695 the investigators were not blinded during experiments nor data analysis.
696

697 **Acknowledgements**

698 We thank all members of the Vander Heiden lab for helpful discussions, Emma Dawson, Grace
699 Wolczanski, and Alejandra Rosario-Crespo for technical assistance and Jessica Spinelli for
700 assistance with using Seahorse equipment during the COVID-19 pandemic. The authors
701 acknowledge support from F30CA268633 (SMC), MSTP T32GM007753 (SMC), T32GM007287
702 (SMC, MBM, ASZ, KLA), the Kosciuszko Foundation (SET), T32GM144273 (HC), NSF DGE-
703 1122374 (KLA), and F31CA271787 (KLA), as well as support to MGVH from the Ludwig Center
704 at MIT, the MIT Center for Precision Cancer Medicine, and the NCI (R35CA242379,
705 R01CA259253, P30CA1405141).
706

707 **Author Contributions**

708 Conceptualization: SMC, MGVH; Intellectual Discussion: SMC, MBM, MGVH; Proliferation rates:
709 SMC, SET, ASZ, HC; Incucyte: SMC, MBM; Viability: SMC, MBM; Kinetic Isotope Tracing: SMC,
710 SET, MBM, HC; Immunoblotting: SMC, SET; NAD+/NADH measurements: SMC, SET; Oxygen
711 consumption: SMC; PHGDH overexpression constructs: KLA; PHGDH overexpression cell line
712 generation: SMC; GOT1, GOT2, and MDH1 KO generation: RC; Writing: SMC and MGVH; Editing:
713 SMC, MBM, SET, ASZ, KLA, MGVH; Funding Acquisition: MGVH
714

715 **Competing Interests**

716 M.G.V.H. discloses that he is or was a scientific advisor for Agios Pharmaceuticals, iTeos
717 Therapeutics, Sage Therapeutics, Pretzel Therapeutics, Lime Therapeutics, Faeth Therapeutics,

718 Droia Ventures, MPM Capital and Auron Therapeutics. All remaining authors declare no
719 competing interests.
720

721 **References**

722 Abbott, K.L., Subudhi, S., Ferreira, R., Gültekin, Y., Steinbuch, S.C., Bin Munim, M., Ramesh,
723 D.L., Honeder, S.E., Kumar, A.S., Wu, M., Hansen, J.A., Shevzov-Zebrun, A., Rashan, E.H.,
724 Eghbalian, K.M., Sivanand, S., Barbeau, A.M., Riedmayr, L.M., Duquette, M., Ali, A., Henning,
725 N., Trojan, S.E., Waite, M., Kunchok, T., Nakano, M.A., Gourgue, F, Ferraro, G.B., Do, B.T.,
726 Spanoudaki, V., Sánchez-Rivera, F.J., Jin, X., Church, G.M., Jain, R.K., Vander Heiden, M.G.
727 (2026). Nutrient requirements of organ-specific metastasis in breast cancer. Nature *649*, 1292-
728 1301. https://doi.org/10.1038/s41586-025-09898-9.
729
730 Alavian, K.N., Beutner, G., Lazrove, E., Sacchetti, S., Park, H.-A., Licznerski, P., Li, H., Nabili,
731 P., Hockensmith, K., Graham, M., Porter, G. A., & Jonas, E. A. (2014). An uncoupling channel
732 within the c-subunit ring of the F1FO ATP synthase is the mitochondrial permeability transition
733 pore. PNAS *111*, 10580–10585. https://doi.org/10.1073/pnas.1401591111.
734
735 Amoedo, N.D., Obre, E., Rossignol, R. (2017). Drug discovery strategies in the field of tumor
736 energy metabolism: Limitations by metabolic flexibility and metabolic resistance to
737 chemotherapy. Biochimica et Biophysica Acta - Bioenergetics *1858*, 674-685.
738 https://doi.org/10.1016/j.bbabio.2017.02.005.
739
740 Apiz Saab, J.J., Dzierozynski, L.N., Jonker, P.B., AminiTabrizi, R., Shah, H., Elena Menjivar, R.,
741 Scott, A.J., Nwosu, Z.C., Zhu, Z., Chen, R.N., Oh, M., Sheehan, C., Wahl, D.R., Rasca di
742 Magliano, M., Lyssiotis, C.A., Macleod, K.F., Weber, C.R., Muir, A. (2023). Pancreatic tumors
743 exhibit myeloid-driven amino acid stress and upregulate arginine biosynthesis. eLife *12*.
744 https://doi.org/10.7554/eLife.81289.
745
746 Baksh, S.C., Todorova, P.K., Gur-Cohen, S., Hurwitz, B., Ge, Y., Novak, J.S.S., Tierney, M.T.,
747 dela Cruz-Racelis, J., Fuchs, E., Finley, L.W.S. (2020). Extracellular serine controls epidermal
748 stem cell fate and tumour initiation. Nature Cell Biology *22*, 779-790.
749 https://doi.org/10.1038/s41556-020-0525-9.
750
751 Banh, R.S., Biancur, D.E., Yamamoto, K., Sohn, A.S.W., Walters, B., Kuljanin, M., Gikandi, A.,
752 Wang, H., Mancias, J.D., Schneider, R.J., Pacold, M.E., Kimmelman, A.C. (2020). Neurons
753 Release Serine to Support mRNA Translation in Pancreatic Cancer. Cell *183*, 1202-1218.
754 https://doi.org/10.1016/j.cell.2020.10.016.
755
756 Bao, X.R., Ong, S.-E., Goldberger, O., Peng, J., Sharma, R., Thompson, D. A., Vafai, S. B.,
757 Cox, A. G., Marutani, E., Ichinose, F., Goessling, W., Regev, A., Carr, S. A., Clish, C. B., &
758 Mootha, V. K. (2016). Mitochondrial dysfunction remodels one-carbon metabolism in human
759 cells. eLife *5*. https://doi.org/10.7554/elife.10575.
760
761 Bertholet, A.M., Chouchani, E. T., Kazak, L., Angelin, A., Fedorenko, A., Long, J. Z., Vidoni, S.,
762 Garrity, R., Cho, J., Terada, N., Wallace, D. C., Spiegelman, B. M., & Kirichok, Y. (2019). H+
763 transport is an integral function of the mitochondrial ADP/ATP carrier. Nature *571*, 515–520.
764 https://doi.org/10.1038/s41586-019-1400-3.

765
766 Birsoy, K., Wang, T., Chen, W.W., Freinkman, E., Abu-Remaileh, M., Sabatini, D.M. (2015). An
767 Essential Role of the Mitochondrial Electron Transport Chain in Cell Proliferation Is to Enable
768 Aspartate Synthesis. Cell *162*, 540-551. https://doi.org/10.1016/j.cell.2015.07.016.
769
770 Broeks, M.H., Meijer, N.W.F., Westland, D., Bosma, M., Gerrits, J., German, H.M., Ciapaite, J.,
771 van Karnebeek, C.D.M., Wanders, R.J.A., Zwartkruis, F.J.T., Verhoeven-Duif, N., Jans, J.J.M.
772 (2023). The malate-aspartate shuttle is important for de novo serine biosynthesis. Cell Reports
773 *42*. https://doi.org/10.1016/j.celrep.2023.113043.
774
775 Buttgereit, F., Brand, M.D. (1995). A hierarchy of ATP-consuming processes in mammalian
776 cells. Biochemical Journal *312*, 163-167. https://doi.org/10.1042/bj3120163.
777
778 Chaneton, B., Hillman, P., Zheng, L., Martin, A.C.L., Maddocks, O.D.K., Chokkathukalam, A.,
779 Coyle, J.E., Jankevics, A., Holding, F.P., Vousden, K.H., Frezza, C., O'Reilly, M., Gottlieb, E.
780 (2012). Serine is a natural ligand and allosteric activator of pyruvate kinase M2. Nature *491*,
781 458-462. https://doi.org/10.1038/nature11540.
782
783 Christensen, C.E., Karlsson, M., Winther, J.R., Jensen, P.R., Lerche, M.H. (2014). Non-invasive
784 In-cell Determination of Free Cytosolic [NAD+]/[NADH] Ratios Using Hyperpolarized Glucose
785 Show Large Variations in Metabolic Phenotypes. Journal of Biological Chemistry *289*, 2344-
786 2352. https://doi.org/10.1074/jbc.M113.498626.
787
788 Cognet, G., Muir, A. (2024). Identifying metabolic limitations in the tumor microenvironment.
789 Science Advances *10*. https://doi.org/10.1126/sciadv.adq7305.
790
791 Deberardinis, R.J., Lum, J.J., Hatzivassiliou, G., Thompson, C.B. (2008). The Biology of
792 Cancer: Metabolic Reprogramming Fuels Cell Growth and Proliferation. Cell Metabolism *7*, 11-
793 20. https://doi.org/10.1016/j.cmet.2007.10.002.
794
795 Delage, B., Fennell, D.A., Nicholson, L., McNeish, I., Lemoine, N.R., Crook, T., Szlosarek, P.W.
796 (2010). Arginine deprivation and argininosuccinate synthetase expression in the treatment of
797 cancer. International Journal of Cancer *126*, 2762-2772. https://doi.org/10.1002/ijc.25202.
798
799 DeNicola, G.M., Chen P., Mullarky E., Sudderth, J.A., Hu, Z., Wu, D., Tang, H., Xie, Y., Asara
800 J.M., Huffman, K.E., Wistuba, I.I., Minna, J.D., DeBerardinis, R.J., Cantley, L.C. (2015). NFR2
801 regulates serine biosynthesis in non-small cell lung cancer. Nature Genetics *47*, 1475-1481.
802 https://doi.org/10.1038/ng.3421.
803
804 Diehl, F.F., Lewis, C.A., Fiske, B.P., Vander Heiden, M.G. (2019). Cellular redox state
805 constrains serine synthesis and nucleotide production to impact cell proliferation. Nature
806 Metabolism *1*, 861-867. https://doi.org/10.1038/s42255-019-0108-x.
807
808 Fantin, V.R., St-Pierre, J., Leder, P. (2006). Attenuation of LDH-A expression uncovers a link
809 between glycolysis, mitochondrial physiology, and tumor maintenance. Cancer Cell *9*, 425-434.
810 https://doi.org/10.1016/j.ccr.2006.04.023.
811
812 Faubert, B., Solmonson, A., Deberardinis, R.J. (2020). Metabolic reprogramming and cancer
813 progression. Science *368*. https://doi.org/10.1126/science.aaw5473.
814

Fendt, S., Frezza, C., Erez, A. (2020). Targeting Metabolic Plasticity and Flexibility Dynamics for Cancer Therapy. Cancer Discovery *10*, 1797-1807. https://doi.org/10.1158/2159-8290.CD-20-0844.

Ferraro, G.B., Ali, A., Luengo, A., Kodack, D.P., Deik, A., Abbott, K.L., Bezwada, D., Blanc, L., Prideaux, B., Jin, X., Possada, J.M., Chen, J., Chin, C.R., Amoozgar, Z., Ferreira, R., Chen, I., Naxerova, K., Ng, C., Westermark, A.M., Duquette, M., Roberge, S., Lindeman, N.I., Lyssiotis, C.A., Nielsen, J., Housman, D.E., Duda, D.G., Brachtel, E., Golub, T.R., Cantley, L.C., Asara, J.M., Davidson, S.M., Fukumua, D., Dartois, V.A., Clish, C.B., Jain, R.K., Vander Heiden, M.G. (2021). Fatty acid synthesis is required for breast cancer brain metastasis. Nature Cancer *2*, 414-428. https://doi.org/10.1038/s43018-021-00183-y.

Fisher-Wellman, K.H., Neufer, P.D. (2012). Linking mitochondrial bioenergetics to insulin resistance via redox biology. Trends in Endocrinology & Metabolism *23*, 142-153. https://doi.org/10.1016/j.tem.2011.12.008.

Gao, X., Lee, K., Reid, M.A., Sanderson, S.M., Qiu, C., Li, S., Liu, J., Locasale, J.W. (2018). Serine Availability Influences Mitochondrial Dynamics and Function through Lipid Metabolism. Cell Reports *22*, 3507-3520. https://doi.org/10.1016/j.celrep.2018.03.017.

Garcia-Bermudez, J., Baudrier, L., La, K., Ge Zhu, X., Fidelin, J., Sviderskiy, V.O., Papagiannakopoulos, T., Molina, H., Snuderl, M., Lewis, C.A., Possemato, R.L., Birsoy, K. (2018). Aspartate is a limiting metabolite for cancer cell proliferation under hypoxia and in tumours. Nature Cell Biology *20*, 775-781. https://doi.org/10.1038/s41556-018-0118-z.

Gibson, G., Blass, J.P. (1976). A Relation between [NAD+]/[NADH] Potentials and Glucose Utilization in Rat Brain Slices. Journal of Biological Chemistry *251* (*13*), 4127-4130.

Gravel, S., Hulea, L., Toban, N., Birman, E., Blouin, M., Zakikhani, M., Zhao, Y., Topisirovic, I., St-Pierre, J., Pollak, M. (2014). Serine Deprivation Enhances Antineoplastic Activity of Biguanides. Cancer Research *74*, 7521-7533. https://doi.org/10.1158/0008-5472.CAN-14-2643-T.

Gullino, P.M., Clark, S.H., Grantham, F.H. (1964). The Interstitial Fluid of Solid Tumors. Cancer Research *24*, 780-797.

Hanahan, D., Weinberg, R.A. (2011). Hallmarks of Cancer: The Next Generation. Cell *144*, 646–674. https://doi.org/10.1016/j.cell.2011.02.013.

Handy, D.E., Loscalzo, J. (2012). Redox Regulation of Mitochondrial Function. Antioxidants & Redox Signaling *16*, 1323-1367. https://doi.org/10.1089/ars.2011.4123.

Holness, M.J., Sugden, M.C. (2003). Regulation of pyruvate dehydrogenase complex activity by reversible phosphorylation. Biochemical Society Transactions *31* (*6*), 1143-1151. https://doi.org/10.1042/bst0311143.

Hosios, A.M., Hecht, V.C., Danai, L.V., Johnson, M.O., Rathmell, J.C., Steinhauser, M.L., Manalis, S.R., Vander Heiden, M.G. (2016). Amino acids rather than glucose account for the majority of cell mass in proliferating mammalian cells. Developmental Cell *36*, 540-549. https://doi.org/10.1016/j.devcel.2016.02.012.

Hosios, A.M., Li, Z., Lien, E.C., Vander Heiden, M.G. (2018). Preparation of Lipid-Stripped Serum for the Study of Lipid Metabolism in Cell Culture. Bio-protocol *8*. https://doi.org/10.21769/BioProtoc.2876

Hosios, A.M., and Vander Heiden, M.G. (2018). The redox requirement of proliferation mammalian cells. Journal of Biological Chemistry *293*, 7490-7498. https://doi.org/10.1074/jbc.TM117.000239.

Krall, A.S., Mullen, P.J., Surjano, F., Momcilovic, M., Schmid, E.W., Halbrook, C.J., Thambundit, A., Mittelman, S.D., Lyssiotis, C.A., Shackelford, D.B., Knott, S.R.V., Christofk, H.R. (2021). Asparagine couples mitochondrial respiration to ATF4 activity and tumor growth. Cell Metabolism *33*, 1013-1026. https://doi.org/10.1016/j.cmet.2021.02.001.

Labuschagne, C.F., van den Broek, N.J.F., Mackay, G.M., Vousden, K.H., Maddocks, O.D.K. (2014). Serine, but not glycine, supports one-carbon metabolism and proliferation of cancer cells. Cell Reports *7*. https://doi.org/10.1016/j.celrep.2014.04.045.

Lapuente-Brun, E., Moreno-Loshuertos, R., Acin-Perez, R., Latorre-Pellicer, A., Colas, C., Balsa, E., Perales-Clemente, E., Quiros, P.M., Calvo, E., Rodriguez-Hernandez, M.A., Navas, P., Cruz, R., Carracedo, A., Lopez-Otin, C., Perez-Martos, A., Fernandez-Silva, P., Fernandez-Vizarra, E., Enriquez, J.A. (2013). Supercomplex Assembly Determines Electron Flux in the Mitochondrial Electron Transport Chain. Science *340*, 1567-1570. https://doi.org/10.1126/science.1230381.

Li, Z., Ji, B.W., Dixit, P.D., Lien, E.C., Tchourine, K., Hosios, A.M., Abbott, K.L., Westermark, A.M., Gorodetsky, E.F., Sullivan, L.B., Vander Heiden, M.G., Vitkup, D. (2022). Cancer cells depend on environmental lipids for proliferation when electron acceptors are limited. Nature Metabolism *4*, 711-723. https://doi.org/10.1038/s42255-022-00588-8.

Locasale, J.W., Grassian, A.R., Melman, T., Lyssiotis, C.A., Mattaini, K.R., Bass, A.J., Heffron, G., Metallo, C.M., Muranen, T., Sharfi, H., Sasaki, A.T., Anastasiou, D., Mullarky, E., Vokes, N.I., Sasaki, M., Beroukhim, R., Stephanopoulos, G., Ligon, A.H., Meyerson, M., Richardson, A.L., Chin, L., Wagner, G., Asara, J.M., Brugge, J.S., Cantley, L.C., Vander Heiden, M.G. (2011). Phosphoglycerate dehydrogenase diverts glycolytic flux and contributes to oncogenesis. Nature Genetics *43*, 869-874. https://doi.org/10.1038/ng.890.

Lopes, E.C., Shi, F., Sawant, A., Ibrahim, M., Gomez-Jenkins, M., Hu, Z., Manchiraju, P., Bhatt, V., Wang, W., Hinrichs, C.S., Wallace, D.C., Su, X., Rabinowitz, J.D., Chan, C.S., Guo, J.Y., Ganesan, S., Lattime, E.C., White, E. (2025). Respiration defects limit serine synthesis required for lung cancer growth and survival. Nature Communications *16*. https://doi.org/10.1038/s41467-025-62911-7.

Luengo, A., Li, Z., Gui, D. Y., Sullivan, L. B., Zagorulya, M., Do, B. T., Ferreira, R., Naamati, A., Ali, A., Lewis, C. A., Thomas, C. J., Spranger, S., Matheson, N. J., & Vander Heiden, M. G. (2021). Increased demand for NAD+ relative to ATP drives aerobic glycolysis. Molecular Cell *81*, 691–707. https://doi.org/10.1016/j.molcel.2020.12.012.

Lyssiotis, C.A., Kimmelman, A.C. (2017). Metabolic Interactions in the Tumor Microenvironment. Trends in Cell Biology *27*, 863-875. https://doi.org/10.1016/j.tcb.2017.06.003.

Maddocks, O.D.K., Athineos, D., Cheung, E. C., Lee, P., Zhang, T., Van Den Broek, N. J. F., Mackay, G. M., Labuschagne, C. F., Gay, D., Kruiswijk, F., Blagih, J., Vincent, D. F., Campbell, K. J., Ceteci, F., Sansom, O. J., Blyth, K., & Vousden, K. H. (2017). Modulating the therapeutic response of tumours to dietary serine and glycine starvation. Nature *544*, 372–376. https://doi.org/10.1038/nature22056.

Maddocks, O.D.K., Berkers, C. R., Mason, S. M., Zheng, L., Blyth, K., Gottlieb, E., & Vousden, K. H. (2013). Serine starvation induces stress and p53-dependent metabolic remodelling in cancer cells. Nature *493* (*7433*), 542–546. https://doi.org/10.1038/nature11743.

McLaughlin, S.G., Dilger, J.P. (1980). Transport of protons across membranes by weak acids. Physiological Reviews *60* (*3*), 825-863. https://doi.org/10.1152/physrev.1980.60.3.825.

Murphy, J.P., Giacomantonio, M. A., Paulo, J. A., Everley, R. A., Kennedy, B. E., Pathak, G. P., Clements, D. R., Kim, Y., Dai, C., Sharif, T., Gygi, S. P., & Gujar, S. (2018). The NAD+ Salvage Pathway Supports PHGDH-Driven Serine Biosynthesis. Cell Reports *24*, 2381–2391.e2385. https://doi.org/10.1016/j.celrep.2018.07.086.

Newman, A.C., Maddocks, O.D.K. (2017). One-carbon metabolism in cancer. British Journal of Cancer *116*, 1499-1504. https://doi.org/10.1038/bjc.2017.118.

Ngo, B., Kim, E., Osorio-Vasquez, V., Doll, S., Bustraan, S., Liang, R. J., Luengo, A., Davidson, S. M., Ali, A., Ferraro, G. B., Fischer, G. M., Eskandari, R., Kang, D. S., Ni, J., Plasger, A., Rajasekhar, V. K., Kastenhuber, E. R., Bacha, S., Sriram, R. K., … Pacold, M. E. (2020). Limited Environmental Serine and Glycine Confer Brain Metastasis Sensitivity to PHGDH Inhibition. Cancer Discovery *10*, 1352–1373. https://doi.org/10.1158/2159-8290.cd-19-1228.

Nobes, C.D., Lakin-Thomas, P.L., Brand, M.D. (1989). The contribution of ATP turnover by the Na+/K+-ATPase to the rate of respiration of hepatocytes: Effects of thyroid status and fatty acids. Biochimica Et Biophysica Acta (BBA) - Bioenergetics *976*, 241-245. https://doi.org/10.1016/S0005-2728(89)80236-1.

Novelli, G.D., Lipmann, F. (1950). The Catalytic Function of Coenzyme A in Citric Acid Synthesis. Journal of Biological Chemistry *182*, 213-228. https://doi.org/10.1016/S0021-9258(18)56541-8.

Patel, M.S., Korotchkina, L.G. (2006). Regulation of the pyruvate dehydrogenase complex. Biochemical Society Transactions *34* (*2*), 217-222. https://doi.org/10.1042/BST20060217.

Pavlova, N.N., Thompson, C.B. (2017). The Emerging Hallmarks of Cancer Metabolism. Cell Metabolism *23*, 27-47. https://doi.org/10.1016/j.cmet.2015.12.006.

Possemato, R., Marks, K.M., Shaul, Y.D., Pacold, M.E., Kim, D., Birsoy, K., Sethumadhavan, S., Woo, H., Jang, H.G., Jha, A.K., Chen, W.W., Barrett, F.G., Stransky, N., Tsun, Z., Cowley, G.S., Barretina, J., Kalaany, N.Y., Hsu, P.P., Ottina, K., Chan, A.M., Yuan, B., Garrayway, L.A., Root, D.E., Mino-Kenudson, M., Brachtel, E.F., Driggers, E.M., Sabatini, D.M. (2011). Functional genomics reveals serine synthesis is essential in PHGDH-amplified breast cancer. Nature *476*, 346-350. https://doi.org/10.1038/nature10350.

Qiu, F., Chen, Y.-R., Liu, X., Chu, C.-Y., Shen, L.-J., Xu, J., Gaur, S., Forman, H. J., Zhang, H., Zheng, S., Yen, Y., Huang, J., Kung, H.-J., & Ann, D. K. (2014). Arginine Starvation Impairs

Mitochondrial Respiratory Function in ASS1-Deficient Breast Cancer Cells. Science Signaling *7*, ra31. https://doi.org/10.1126/scisignal.2004761.

Rabinovich, S., Adler, L., Yizhak, K., Sarver, A., Silberman, A., Agron, S., Stettner, N., Sun, Q., Brandis, A., Helbling, D., Korman, S., Itzkovitz, S., Dimmock, D., Ulitsky, I., Nagamani, S. C. S., Ruppin, E., & Erez, A. (2015). Diversion of aspartate in ASS1-deficient tumours fosters de novo pyrimidine synthesis. Nature *527*, 379-383. https://doi.org/10.1038/nature15529.

Sciacovelli, M., Dugourd, A., Valcarcel Jimenez, L., Yang, M., Nikitopoulou, E., Costa, A.S.H., Tronci, L., Caraffini, V., Rodrigues, P., Schmidt, C., Gerard Ryan, D., Young, T., Zecchini, V.R., Rossi, S.H., Massie, C., Lohoff, C., Masid, M., Hatzimanikatis, V., Kuppe, C., Kriegsheim, A.V., Kramann, R., Gnanapragasam, V., Warren, A.Y., Stewart, G.D., Erez, A., Vanharanta, S., Saez-Rodriguez, J., Frezza, C. (2022). Dynamic partitioning of branched-chain amino acids-derived nitrogen supports renal cancer progression. Nature Communications *13* (*7830*). https://doi.org/10.1038/s41467-022-35036-4.

Sivanand, S., Gultekin, Y., Winter, P.S., Vermeulen, S.Y., Tchourine, K.M., Abbott, K.L., Danai, L.V., Gourge, F., Do, B.T., Crowder, K., Kunchok, T., Lau, A.N., Darnell, A.M., Jefferson, A., Morita, S., Duda, D.G., Aguirre, A.J., Wolpin, B.M., Henning, N., Spanoudaki, V., Maiorino, L., Irvine, D.J., Yilmaz, O.H., Lewis, C.A., Vitkup, D., Shalek, A.K., Vander Heiden, M.G. (2024). Cancer tissue of origin constrains the growth and metabolism of metastases. Nature Metabolism *6*, 1668-1681. https://doi.org/10.1038/s42255-024-01105-9.

Srere, P.A. (1974). Controls of citrate synthase activity. Life Sciences *15*, 1695-1710. https://doi.org/10.1016/0024-3205(74)90172-6.

Sullivan, L.B., Gui, D.Y., Hosios, A.M., Bush, L.N., Freinkman, E., Vander Heiden M.G. (2015). Supporting Aspartate Biosynthesis Is an Essential Function of Respiration in Proliferation Cells. Cell *162*, 552-563. https://doi.org/10.1016/j.cell.2015.07.017.

Sullivan, M.R., Danai, L. V., Lewis, C. A., Chan, S. H., Gui, D. Y., Kunchok, T., Dennstedt, E. A., Vander Heiden, M. G., Muir, A. (2019a). Quantification of microenvironmental metabolites in murine cancers reveals determinants of tumor nutrient availability. eLife *8*. https://doi.org/10.7554/elife.44235.

Sullivan, M.R., Mattaini, K.R., Dennstedt, E.A., Nguyen, A.A., Reilly, M.F., Meeth, K., Muir, A., Darnell, A.M., Bosenberg, M.W., Lewis, C.A., Vander Heiden, M.G. (2019b). Increased serine synthesis provides an advantage for tumors arising in tissues where serine levels are limiting. Cell Metabolism *29*, 1410-1421,e1414. https://doi.org/10.1016/j.cmet.2019.02.015.

Terada, H. (1990). Uncouplers of Oxidative Phosphorylation. Environmental Health Perspectives *87*, 213-218. https://doi.org/10.1289/ehp.9087213.

Titov, D.V., Cracan, V., Goodman, R. P., Peng, J., Grabarek, Z., & Mootha, V. K. (2016). Complementation of mitochondrial electron transport chain by manipulation of the NAD+/NADH ratio. Science *352*, 231-235. https://doi.org/10.1126/science.aad4017.

Vander Heiden, M.G., Chandel, N.S., Schumacker, P.T., Thompson, C.B. (1999). Bcl-xL Prevents Cell Death following Growth Factor Withdrawal by Facilitating Mitochondrial ATP/ADP Exchange. Molecular Cell *3*, 159-167. https://doi.org/10.1016/S1097-2765(00)80307-X.

1018 Vander Heiden, M.G., Deberardinis R.J. (2017). Understanding the Intersections between
1019 Metabolism and Cancer Biology. Cell *168*, 657-669. https://doi.org/10.1016/j.cell.2016.12.039.
1020
1021 Vichai, V., Kirtikara, K. (2006). Sulforhodamine B colorimetric assay for cytotoxicity screening.
1022 Nature Protocols *1*, 1112-1116. https://doi.org/10.1038/nprot.2006.179.
1023
1024 Wang, Y., Stancliffe, E., Fowle-Grider, R., Wang, R., Wang, C., Schwaiger-Haber, M., Shriver,
1025 L.P., Patti, G.J. (2022). Saturation of the mitochondrial NADH shuttles drives aerobic glycolysis
1026 in proliferating cells. Molecular Cell *82*, 3270-3283. https://doi.org/10.1016/j.molcel.2022.07.007.
1027
1028 Wu, Z., Bezwada, D., Cai, F., Harris, R.C., Ko, B., Sondhi, V., Pan, C., Vu, H.S., Nguyen, P.T.,
1029 Faubert, B., Cai, L., Chen, H., Martin-Sandoval, M., Do, D., Gu, W., Zhang, Y., Zhang, Y.,
1030 Brooks, B., Kelekar, S., Zacharias, L.G., Oaxaca, K.C., Patricio, J.S., Mathews, T.P., Garcia-
1031 Bermudez, J., Ni, M., DeBerardinis, R.J., (2024). Electron transport chain inhibition increases
1032 cellular dependence on purine transport and salvage. Cell Metabolism *36*, 1504-1520.
1033 https://doi.org/10.1016/j.cmet.2024.05.014.
1034
1035 Xiao, Y., Yu, T., Xu, Y., Ding, R., Wang, Y., Jiang, Y., Shao, Z. (2023). Emerging therapies in
1036 cancer metabolism. Cell Metabolism *35*, 1283-1303. https://doi.org/10.1016/j.cmet.2023.07.006.
1037
1038 Yao, C., Wang, R., Wang, Y., Kung, C., Weber, J.D., Patti, G.J. (2019). Mitochondrial fusion
1039 supports increased oxidative phosphorylation during cell proliferation. eLife *8*.
1040 https://doi.org/10.7554/eLife.41351.
1041
1042 Zhao, R., Jiang, S., Zhang, L., Yu, Z. (2019). Mitochondrial electron transport chain, ROS
1043 generation, and uncoupling International Journal of Molecular Medicine *44*, 3-15.
1044 https://doi.org/10.3892/ijmm.2019.4188.
1045

1046 **Figure Legends**

1047 **Figure 1. The NAD+/NADH ratio is proportional to serine synthesis rate. (A)** α-ketobutyrate
1048 (AKB) is an exogenous electron acceptor that promotes the oxidation of NADH into NAD+ through
1049 its conversion to α-hydroxybutyrate (AHB). Rotenone inhibits activity of complex I of the
1050 mitochondrial electron transport chain (ETC) to block NADH oxidation into NAD+. **(B)**
1051 NAD+/NADH ratio measured in A549 cells cultured without serine and indicated concentrations
1052 of AKB (left) and rotenone (right) for 24 hours. NAD+/NADH ratios are normalized to untreated
1053 cells cultured without serine, n=3. Pearson correlation coefficients and P-values were calculated
1054 by simple linear regression, ***$p<0.005$, ****$p<0.001$. **(C)** Schematic depicting NAD+ requirement
1055 to produce serine labeled (M+3) from U-^{13}C-glucose. Under culture conditions without serine,
1056 intracellular serine rapidly effluxes from cells into culture media. Thus, cells and media were jointly

1057 analyzed at each time point of kinetic tracing to better capture levels of newly synthesized serine.
1058 **(D)** Serine labeled (M+3) from U-^{13}C-glucose over time in A549 cells cultured without serine and
1059 with indicated concentrations of AKB or rotenone for 24 hours prior to U-^{13}C-glucose exposure.
1060 Serine levels are normalized to internal norvaline standard and cell number measured in indicated
1061 conditions, n=3. **(E)** Relative NAD+/NADH ratios from A549 cells cultured without serine after
1062 exposure to 250 μM AKB, 1000 μM AKB, 20 nM rotenone, or 40 nM rotenone for 24 hours are
1063 plotted against the serine synthesis rates from corresponding conditions as shown in (D). Serine
1064 synthesis rates are calculated from labeled serine (M+3) after 1 and 15 minutes of U-^{13}C-glucose
1065 exposure and normalized to untreated culture conditions without serine, n=3. Pearson correlation
1066 coefficients and P-values were calculated by simple linear regression, ****$p<0.001$. Data shown
1067 for all panels represent mean ± SD.
1068
1069 **Figure 2. The NAD+/NADH ratio differs between cancer cells upon serine withdrawal and**
1070 **correlates with proliferation in serine depleted conditions. (A)** Proliferation rate (doublings
1071 per day) of indicated cancer cells cultured without serine for 72 hours normalized to proliferation
1072 rate of corresponding cancer cells cultured with serine, n=3. **(B)** NAD+/NADH ratios of indicated
1073 cells cultured with or without serine for 24 hours. Yellow indicates cells with unaltered
1074 NAD+/NADH ratios (redox non-responder cells) and blue indicates cells with elevated
1075 NAD+/NADH ratios when cultured without serine (redox responder cells). Values are normalized
1076 to the NAD+/NADH ratios of cells cultured with serine, n=3. P-values were calculated by unpaired
1077 Student's t-test, **$p<0.01$, ***$p<0.005$. **(C)** Relative NAD+/NADH ratios of cells cultured without
1078 serine are plotted against proliferation rates of corresponding cells cultured without serine. Data
1079 points are labeled to denote the different cell lines (Calu6, A549, 8988T, MIA PaCa-2, H1299,
1080 and HCT116). Pearson correlation coefficient and P-values were calculated by simple linear
1081 regression, *$p<0.05$. **(D)** Serine labeled (M+3) from U-^{13}C-glucose over time in A549 and H1299
1082 cells cultured with or without serine for 24 hours prior to U-^{13}C-glucose exposure. Serine levels

1083 were normalized to internal norvaline standard and cell number measured in indicated conditions,
1084 n=3. **(E)** Absolute fold change of serine labeled (M+3) from U-^{13}C-glucose in A549 and H1299
1085 cells cultured without serine relative to serine labeled (M+3) from U-^{13}C-glucose in A549 and
1086 H1299 cells cultured with serine for 24 hours after 12 minutes of U-^{13}C-glucose exposure, n=3.
1087 P-values were calculated by unpaired Student's t-test, **p<0.01. Data shown for all panels are
1088 means ± SD.
1089
1090 **Figure 3. Elevated mitochondrial respiration is associated with increased NAD+/NADH**
1091 **ratios and serine synthesis rates. (A)** Oxygen consumption rate (OCR) of indicated cells
1092 cultured with or without serine for 24 hours. Values are averages of three repeat measurements,
1093 n=14-20. P-values were calculated by unpaired Student's t-test, *p<0.05, ****p<0.001. **(B)** OCR
1094 of cells (H1299 top, A549 bottom) cultured with indicated concentrations of serine for 24 hours.
1095 Values are averages of three repeat measurements, n=3-9. P-values were calculated by unpaired
1096 Student's t-test, ****p<0.001. **(C)** NAD+/NADH ratios of cells (H1299 top, A549 bottom) cultured
1097 with indicated concentrations of serine for 24 hours. Values are normalized to the NAD+/NADH
1098 ratio of cells cultured in 400 μM serine (serine concentration in DMEM), n=3. P-values were
1099 calculated by unpaired Student's t-test, **p<0.01, ***p<0.005. **(D)** Relative OCR plotted against
1100 relative NAD+/NADH ratios in H1299 and A549 cells cultured in 0, 25, 50, and 100 μM serine for
1101 24 hours. OCR and NAD+/NADH ratios are normalized to measurements from the 100 μM serine
1102 condition, n=3. Pearson correlation coefficients and P-values were calculated by simple linear
1103 regression, *p<0.05, ****p<0.001. **(E)** Serine labeled (M+3) from U-^{13}C-glucose over time in cells
1104 (H1299 top, A549 bottom) cultured with indicated serine concentrations for 24 hours prior to U-
1105 ^{13}C-glucose exposure. Serine levels are normalized to internal norvaline standard and cell number
1106 measured in indicated conditions, n=3. **(F)** Relative NAD+/NADH ratios of cells (H1299 top, A549
1107 bottom) cultured with 0, 25, 50, and 100 μM serine for 24 hours plotted against relative serine
1108 synthesis rates of cells cultured in corresponding conditions. Serine synthesis rates are calculated

1109 from labeled serine (M+3) after 1 and 15 minutes of U-^{13}C-glucose exposure and normalized to
1110 untreated culture conditions without serine, n=3. Pearson correlation coefficients and P-values
1111 were calculated by simple linear regression, ***p<0.005. Data shown for all panels are means ±
1112 SD.
1113
1114 **Figure 4. Mitochondrial respiration governs the endogenous cell NAD+/NADH ratio and**
1115 **influences serine synthesis. (A)** Schematic depicting the mitochondrial electron transport chain
1116 (ETC) and the protonophore activity of FCCP that uncouples the ETC from ATP synthase activity.
1117 CoQ(H_2) indicates the oxidized and reduced (H_2) forms of coenzyme Q, cyt_c denotes cytochrome
1118 c. **(B,C)** Proliferation rate (doublings per day) of A549 (B) and H1299 cells (C) cultured with or
1119 without serine with indicated concentrations of FCCP for 72 hours, n=3. Increasing doses of FCCP
1120 statistically increased proliferation of A549 cells cultured without serine (p<0.001). P-values were
1121 calculated by simple linear regression. **(D)** Serine labeled (M+3) from U-^{13}C-glucose over time in
1122 A549 cells without serine and with or without 2 μM FCCP treatment for 24 hours prior to U-^{13}C-
1123 glucose exposure. Serine levels are normalized to internal norvaline standard and cell number
1124 measured in indicated conditions, n=3. **(E)** Serine labeled (M+3) from U-^{13}C-glucose over time in
1125 H1299 cells without serine, and with or without 2 μM FCCP treatment for 24 hours prior to U-^{13}C-
1126 glucose exposure. Serine levels are normalized to internal norvaline standard and cell number
1127 measured in indicated conditions, n=3. **(F)** Oxygen consumption rate (OCR) of A549 cells cultured
1128 with or without serine with indicated FCCP treatment for 24 hours. Values are averages of three
1129 repeat measurements, n=5-9. P-values were calculated by unpaired Student's t-test, ****p<0.001.
1130 **(G)** Relative NAD+/NADH ratio of A549 cells cultured with or without serine with indicated FCCP
1131 treatment for 24 hours. NAD+/NADH ratios are normalized to the NAD+/NADH ratio in A549 cells
1132 cultured with serine, n=3. P-values were calculated by unpaired Student's t-test, *p<0.05,
1133 ***p<0.005. **(H)** Proliferation rate (doublings per day) of A549 cells cultured with or without serine,
1134 2 μM FCCP, and indicated concentrations of rotenone for 72 hours, n=3. P-values were calculated

1135 by unpaired Student's t-test, *p<0.05. **(I)** Serine labeled (M+3) from U-^{13}C-glucose over time in
1136 A549 cells cultured without serine and with or without 2 μM FCCP or 20 nM rotenone as indicated
1137 for 24 hours prior to U-^{13}C-glucose exposure. Serine levels are normalized to internal norvaline
1138 standard and cell number measured in indicated conditions, n=3. **(J)** Relative NAD+/NADH ratio
1139 of A549 cells cultured with or without serine, 2 μM FCCP, or 20 nM rotenone as indicated.
1140 NAD+/NADH ratios are normalized to the NAD+/NADH ratio in A549 cells cultured with serine,
1141 n=3. P-values were calculated by unpaired Student's t-test, **p<0.01, ***p<0.005. Data shown for
1142 all panels are means ± SD.
1143
1144 **Figure 5. Lipid depletion enhances cell-specific elevation in mitochondrial respiration**
1145 **and the NAD+/NADH ratio, influencing oxidative citrate and serine synthesis. (A)**
1146 Schematic depicting glucose and glutamine oxidative routes for synthesizing citrate, highlighting
1147 NAD+ requiring oxidation reactions. **(B)** Citrate labeled (M+2) from U-^{13}C-glucose over time in
1148 A549 and H1299 cells cultured with or without serine for 24 hours prior to U-^{13}C-glucose
1149 exposure. Citrate levels are normalized to internal norvaline standard and cell number
1150 measured in indicated conditions, n=3. **(C)** Citrate labeled (M+2) from U-^{13}C-glucose over time
1151 in A549 and H1299 cells cultured without serine and with or without 2 μM FCCP for 24 hours
1152 prior to U-^{13}C-glucose exposure. Citrate levels are normalized to internal norvaline standard and
1153 cell number measured in indicated conditions, n=3. **(D)** Citrate labeled (M+2) from U-^{13}C-
1154 glucose over time in A549 cells cultured with serine and with indicated treatment conditions for
1155 24 hours prior to U-^{13}C-glucose exposure. Citrate levels are normalized to internal norvaline
1156 standard and cell number measured in indicated conditions, n=3. **(E)** Oxygen consumption rate
1157 (OCR) in A549 and H1299 cells cultured with or without lipids for 24 hours. Values are averages
1158 of three repeat measurements, n=10. Green indicates lipid redox responder cells. Purple
1159 indicates lipid redox non-responder cells. **(F)** Relative NAD+/NADH ratios of A549 and H1299
1160 cells cultured with or without lipids for 24 hours. NAD+/NADH ratios are normalized to the

1161 NAD+/NADH ratio of the corresponding cell type cultured with lipids, n=3. P-values were
1162 calculated by unpaired Student's t-test, *p<0.05. **(G)** Citrate labeled (M+2) from U-^{13}C-glucose
1163 over time in A549 and H1299 cells cultured with or without lipids for 24 hours prior to U-^{13}C-
1164 glucose exposure. Citrate levels are normalized to internal norvaline standard and cell number
1165 measured in indicated conditions, n=3. **(H)** Serine labeled (M+3) from U-^{13}C-glucose over time
1166 in A549 and H1299 cells cultured with or without lipids for 24 hours prior to U-^{13}C-glucose
1167 exposure. Serine levels are normalized to internal norvaline standard and cell number
1168 measured in indicated conditions, n=3. Data shown for all panels are means ± SD.
1169

1170 **Figure 6. Lipid depletion increases mitochondrial respiration and the NAD+/NADH ratio in**
1171 **a cell-specific manner to influence serine synthesis and proliferation in serine depleted**
1172 **conditions. (A)** Oxygen consumption rate (OCR) of A549 and H1299 cells cultured with or without
1173 serine or lipids for 24 hours. Values are the average of three repeat measurements, n=14-15. P-
1174 values were calculated by one-way ANOVA followed by post-hoc Tukey HSD test, ****p<0.001.
1175 **(B)** Relative NAD+/NADH ratios of A549 and H1299 cells cultured with or without serine or lipids
1176 for 24 hours. NAD+/NADH ratio is normalized to the NAD+/NADH ratio in corresponding cells
1177 cultured with serine and lipids, n=3. P-values were calculated by one-way ANOVA followed by
1178 post-hoc Tukey HSD test, *p<0.05, ****p<0.001. **(C, D)** Left: Serine labeled (M+3) from U-^{13}C-
1179 glucose over time in A549 cells (C) and H1299 cells (D) cultured without serine and with or without
1180 lipids for 24 hours prior to U-^{13}C-glucose exposure. Right: Serine synthesis rates of A549 cells (C)
1181 and H1299 cells (D) cultured in indicated conditions. Serine synthesis rates are calculated from
1182 labeled serine (M+3) after 1 and 15 minutes of U-^{13}C-glucose exposure and normalized to the
1183 serine synthesis rates of the corresponding cell line cultured without serine and with lipids. Serine
1184 levels are normalized to internal norvaline standard and cell number measured in indicated
1185 conditions, n=3. Single data point (H1299, -serine +lipid, t=15 min) removed due to detection error
1186 with no signal. (**E,F)** Left: Citrate labeled (M+2) from U-^{13}C-glucose over time in A549 cells (E)

1187 and H1299 cells (F) cultured without lipids and with or without serine for 24 hours prior to U-^{13}C-
1188 glucose exposure. Right: Citrate synthesis rates of A549 cells (E) and H1299 cells (F) cultured in
1189 indicated conditions. Citrate synthesis rates are calculated from labeled citrate (M+2) after 1 and
1190 15 minutes of U-^{13}C-glucose exposure and normalized to the citrate synthesis rates of the
1191 corresponding cell line cultured without lipids and with serine. Citrate levels are normalized to
1192 internal norvaline standard and cell number measured in indicated conditions, n=3. **(G)**
1193 Proliferation rate (doublings per day) of A549 cells cultured with or without serine or lipids for 72
1194 hours, n=3. P-values were calculated by one-way ANOVA followed by post-hoc Tukey HSD test,
1195 **$p<0.01$ **(H)** Proliferation rate (doublings per day) of H1299 cells cultured with or without serine
1196 or lipids for 72 hours, n=3. Data shown for all panels are means ± SD.
1197
1198 **Figure 7. The cell NAD+/NADH ratio is regulated in a cancer cell-specific manner by**
1199 **changes to mitochondrial respiration in response to nutrient availability, impacting**
1200 **oxidative biosynthetic reactions. (A)** In serine and lipid-replete conditions, cells can acquire
1201 environmental serine and lipids to support proliferation. Cells can also oxidize glucose to produce
1202 serine, as well as citrate for lipid synthesis. The oxidation reactions involved can be limited by
1203 NAD+ availability, which is impacted by mitochondrial respiration. **(B)** In nutrient depleted
1204 conditions, the ability to support oxidative reactions is dependent on the mitochondrial response
1205 to the nutrient depletion. For redox responders, environmental depletion of serine or lipids
1206 increases the cell NAD+/NADH ratio to support both oxidative citrate and serine synthesis. This
1207 ability to increase respiration enables proliferation in conditions lacking serine. **(C)** In redox non-
1208 responder cells, neither mitochondrial respiration nor the NAD+/NADH ratio increases following
1209 nutrient depletion. This limits oxidative synthesis of serine (and citrate), subsequently limiting
1210 proliferation in environments that lack serine.
1211
1212
1213

Supplementary Material

Supplementary Figure 1

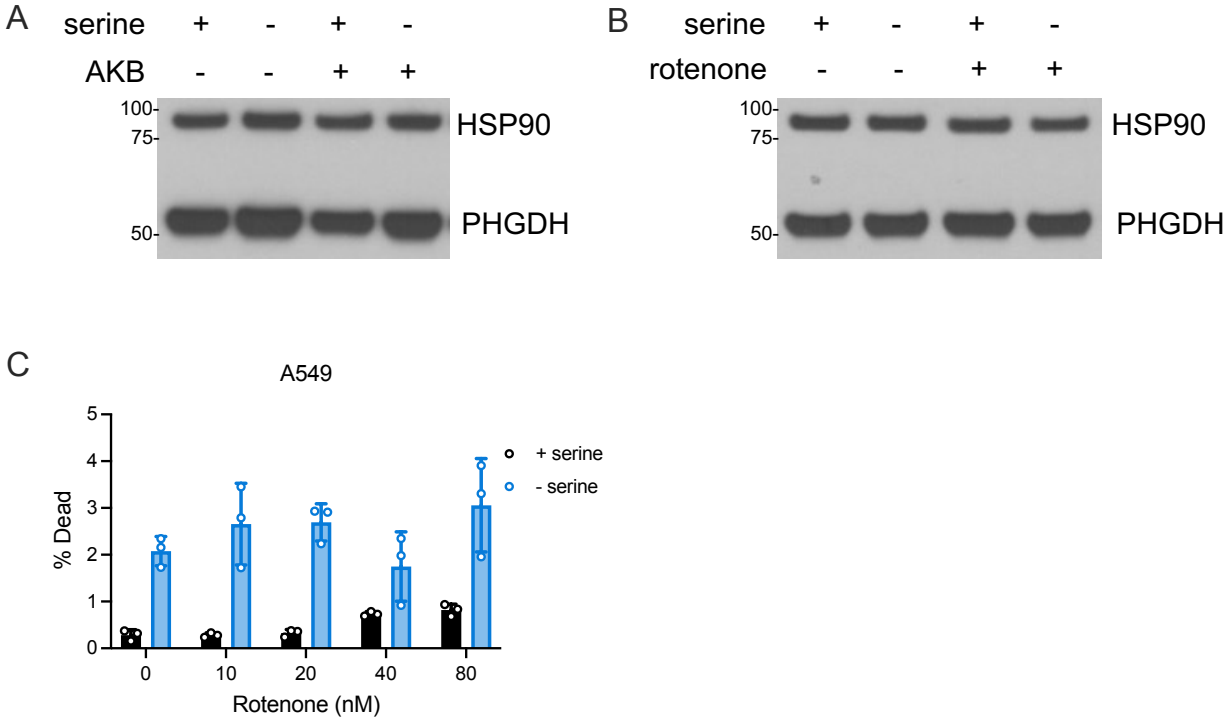

Supplementary Figure 1. Altering NAD+/NADH with α-ketobutyrate (AKB) or rotenone does not change PHGDH protein levels and minimally changes cell viability. (A,B) Immunoblots assessing PHGDH protein levels in A549 cells cultured with or without serine, 1 mM AKB (A), or 20 nM rotenone (B), as indicated for 24 hours. HSP90 expression is shown as a loading control. **(C)** Percent of A549 cells dead, measured using dye exclusion 72 hours after exposure to the indicated concentrations of rotenone in serine-replete or serine depleted conditions, n=3. Serine depletion led to a statistically significant increase in cell death compared to serine-replete conditions at all concentrations of rotenone with the exception of 40 nM rotenone, $p<0.05$. There was no statistical difference in cell death between 0 and 20 nM rotenone in either serine-replete or serine depleted conditions. P-values were calculated using unpaired Student's t-test. Data shown are means ± SD.

Supplementary Figure 2

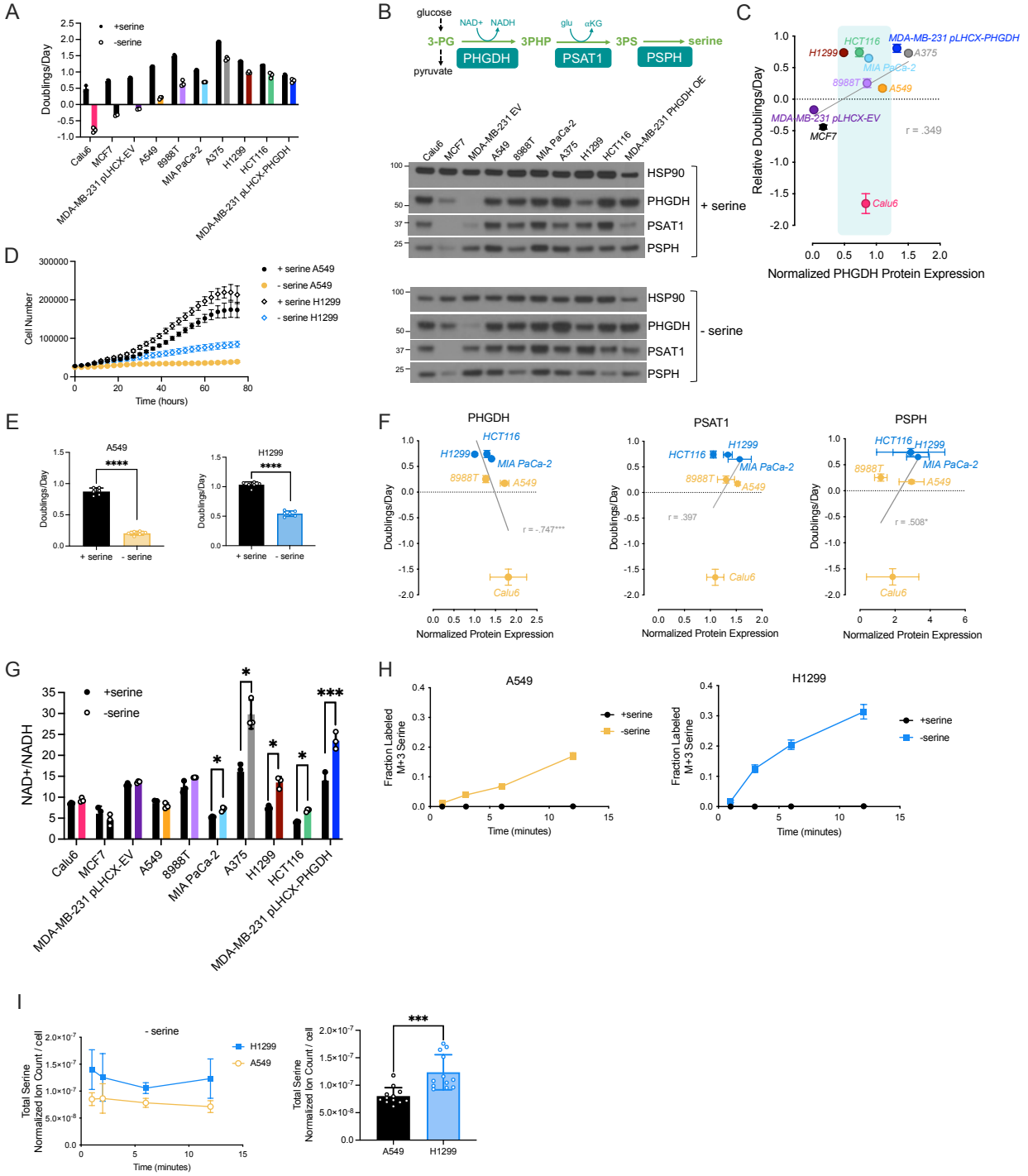

Supplementary Figure 2. Relationship between PHGDH protein expression, cell NAD+/NADH ratio, and cell proliferation rate following serine deprivation. (A) Proliferation rates (doublings per day) of cells cultured with or without serine for 72 hours, n=3. **(B)** Above: Schematic of the serine synthesis pathway. Below: Immunoblot assessing protein levels of PHGDH, PSAT1, and PSPH in the indicated cells cultured with or without serine for 24 hours.

HSP90 protein expression is shown as a loading control. These data are representative of three independent experiments. Abbreviations – 3-PG: 3-phosphoglycerate, PHGDH: phosphoglycerate dehydrogenase, 3PHP: 3-phosphohydroxypyruvate, glu: glutamate, αKG: α-ketoglutarate, PSAT1: phosphoserine aminotransferase 1, 3PS: 3-phosphoserine, PSPH: phosphoserine phosphatase**. (C)** Quantification of PHGDH protein expression for the indicated cells under serine depleted conditions (normalized to HSP90 protein expression) from three biological replicates, correlated with the corresponding relative proliferation rate of indicated cells under serine depleted conditions based on data presented in (A). Cell lines enclosed in the light blue shaded box indicate cancer cell lines with serine synthesis enzyme expression that could not fully predict proliferation in the absence of serine that we chose to examine further. Pearson correlation coefficient calculated by simple linear regression. **(D)** Cell number over time for either A549 cells (yellow) or H1299 cells (blue) in either serine-replete or serine depleted conditions, n=6. **(E)** Calculated doublings per day from the data in (D) for the indicated cells and conditions, n=6. P-values were calculated using unpaired Student's t-test, ****$p<0.001$. **(F)** Correlation between the protein expression of serine synthesis enzymes PHGDH, PSAT1, and PSPH across three biological replicates and proliferation rate in serine depleted conditions for the indicated cell lines, n=3. Pearson correlation coefficient and P-values were calculated by simple linear regression, *$p<0.05$, ***$p<0.005$. **(G)** Unnormalized NAD+/NADH ratios measured for the indicated cell lines cultured with or without serine for 24 hours, n=3 per each cell line. P-values were calculated by unpaired Student's t-test, *$p<0.05$, ***$p<0.005$. **(H)** Fraction of total serine labeled from U-^{13}C-glucose over time in A549 and H1299 cells that were cultured with or without serine for 24 hours prior to U-^{13}C-glucose exposure as indicated, n=3. **(I)** Left: Total intracellular serine levels over time from the kinetic tracing with A549 and H1299 cells cultured with or without serine for 24 hours prior to U-^{13}C-glucose exposure as described in (H). Right: Average of total intracellular serine levels from all time points of the kinetic U-^{13}C-glucose isotope tracing experiment shown in (H). Serine levels were normalized to internal norvaline standard and cell number. P-values were calculated by unpaired Student's t-test, ***$p<0.005$. Data shown for all panels are means ± SD.

Supplementary Figure 3

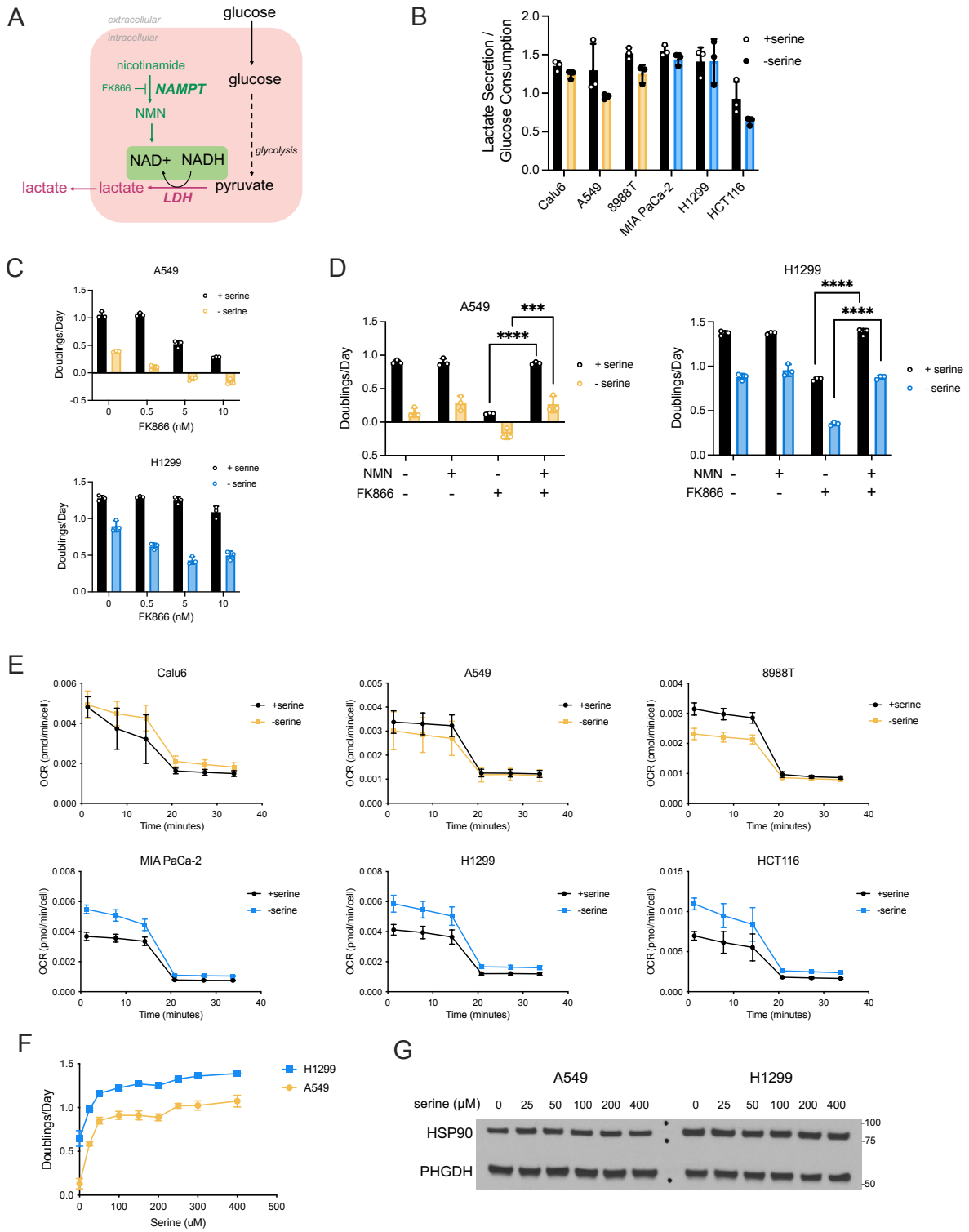

Supplementary Figure 3. Lactate dehydrogenase activity, reliance on the NAD+ salvage pathway, mitochondrial respiration, and PHGDH protein levels following serine deprivation. (A) Schematic depicting the contributions of lactate dehydrogenase (LDH) and the NAD+ salvage

pathway to NAD+ generation. Glucose is consumed by cells and converted to pyruvate via glycolysis. LDH can convert pyruvate to lactate by oxidizing NADH to NAD+. In the NAD+ salvage pathway, nicotinamide can be converted to nicotinamide mononucleotide (NMN) by the enzyme nicotinamide phosphoribosyltransferase (NAMPT), which is inhibited by the small molecule FK866. NMN is subsequently converted to NAD+ via NMN adenylyltransferase. **(B)** Lactate secretion rate normalized to glucose consumption rate as measured in the indicated cells cultured with or without serine for 72 hours, n=3. **(C)** Proliferation rate (doublings per day) of A549 (above) and H1299 cells (below) cultured with or without serine and with or without the indicated concentrations of FK866 for 72 hours, n=3. There was a statistically significant difference in the sensitivity of A549 and H1299 cells to FK866 in the serine-replete condition ($p<0.001$), but not in the serine depleted conditions. P-values were calculated by ANCOVA analysis followed by post-hoc Tukey HSD test. **(D)** Proliferation rate (doublings per day) of A549 (left) and H1299 cells (right) cultured with or without serine and either NMN (100 μM) or FK866 (10 μM) as indicated for 72 hours, n=3. P-values were calculated using unpaired Student's t-test, ***$p<0.005$, ****$p<0.001$. **(E)** Oxygen consumption rate (OCR) of cells cultured with or without serine for 24 hours, n=10-20. Rotenone and antimycin A were injected between the third and fourth OCR measurements to define non-mitochondrial OCR. Data shown are normalized to cell number. **(F)** Proliferation rate (doublings per day) of A549 and H1299 cells cultured in media with the indicated concentrations of serine for 72 hours. Media was replenished every day to avoid serine depletion in lower serine-containing conditions, n=3. **(G)** Immunoblot assessing PHGDH protein levels in A549 or H1299 cells cultured in media with the indicated concentrations of serine for 24 hours. HSP90 expression is shown as a loading control. Data shown for all panels are means ± SD.

Supplementary Figure 4

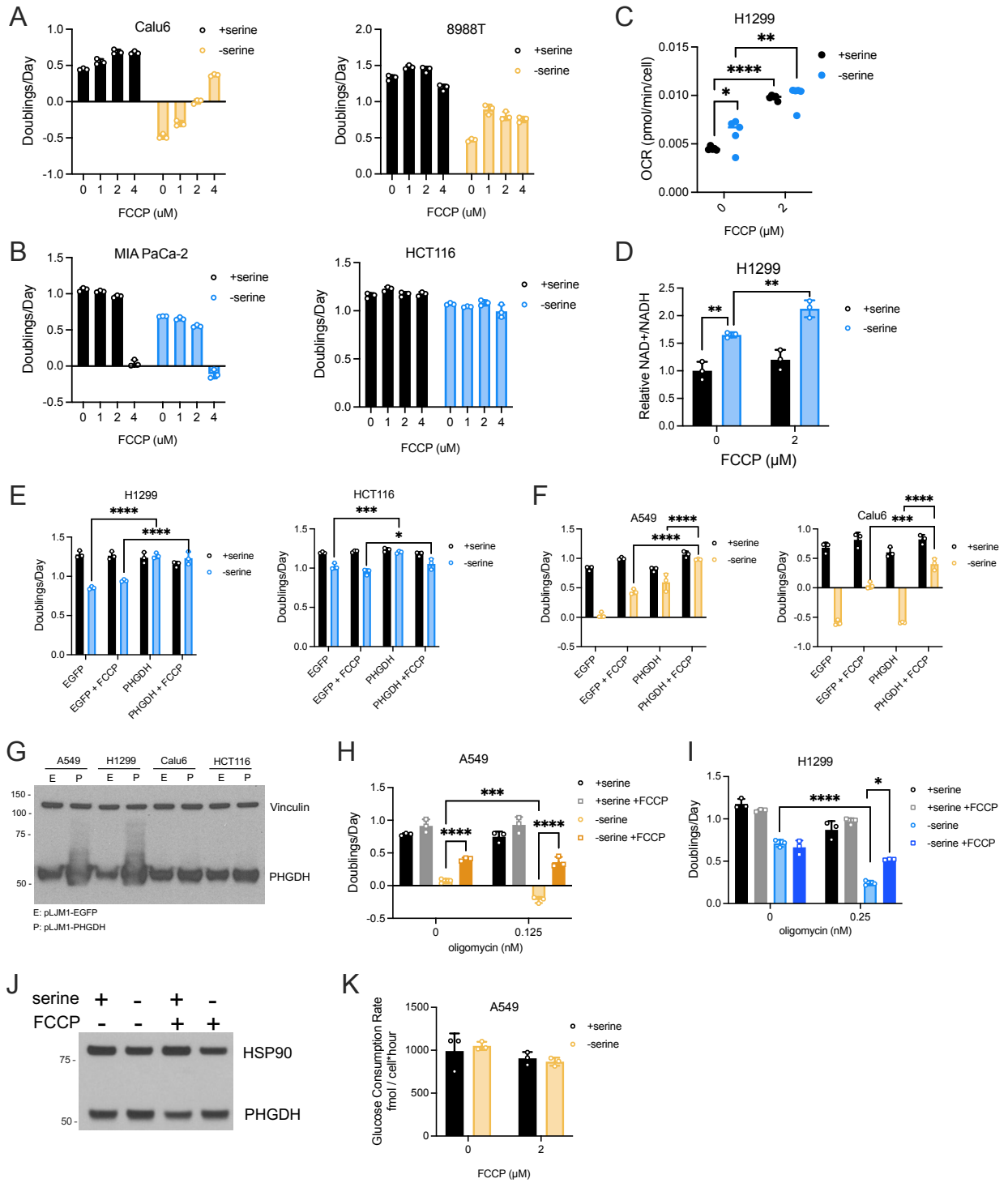

Supplementary Figure 4. FCCP increases both serine synthesis and proliferation of redox non-responder cells in serine depleted conditions. (A) Proliferation rate (doublings per day) of redox non-responder cells Calu6 and 8988T cultured with or without serine and the indicated concentration of FCCP for 72 hours, n=3. Increasing doses of FCCP statistically increased the proliferation of Calu6 cells cultured without serine, $p<0.001$. P-values were calculated by simple

linear regression. All doses of FCCP statistically increased the proliferation of 8988T cells cultured without serine but not in a dose-dependent manner, $p<0.001$. P-values were calculated by unpaired Student's t-test. **(B)** Proliferation rate (doublings per day) of redox responder cells MIA PaCa-2 and HCT116 cultured with or without serine and the indicated concentration of FCCP for 72 hours, n=3. **(C)** Mitochondrial oxygen consumption rate (OCR) of H1299 cells cultured with or without serine and the indicated concentration of FCCP for 24 hours, n=5. Values are averages of three repeat measurements. P-values were calculated by unpaired Student's t-test, *$p<0.05$, **$p<0.01$, ****$p<0.001$. **(D)** NAD+/NADH ratio measured in H1299 cells cultured with or without serine and the indicated concentration of FCCP for 24 hours, n=3. P-values were calculated by unpaired Student's t-test, **$p<0.01$. **(E)** Proliferation rate (doublings per day) of redox responder cells H1299 and HCT116 with or without PHGDH overexpression and cultured with or without serine and 2 μM FCCP, as indicated, for 72 hours, n=3. P-values were calculated by two-way ANOVA followed by post-hoc Tukey HSD test, *$p<0.05$, ***$p<0.005$, ****$p<0.001$. **(F)** Proliferation rate (doublings per day) of redox non-responder cells A549 and Calu6 with or without PHGDH overexpression and cultured with or without serine and 2 μM FCCP for 72 hours, n=3. P-values were calculated by two-way ANOVA followed by post-hoc Tukey HSD test, ***$p<0.005$, ****$p<0.001$. **(G)** Immunoblot assessing PHGDH protein levels in the indicated cell lines without (pLJM1-EGFP) or with (pLJM1-PHGDH) exogenous PHGDH expression. Vinculin expression is shown as a loading control. **(H,I)** Proliferation rate (doublings per day) of A549 cells (H) and H1299 cells (I) cultured with or without serine, with or without 2 μM FCCP, or the indicated concentration of oligomycin for 72 hours, n=3. P-values were calculated by unpaired Student's t-test, *$p<0.05$, ***$p<0.005$, ****$p<0.001$. **(J)** Immunoblot assessing PHGDH protein levels in A549 cells cultured with or without serine and with or without 2 μM FCCP for 24 hours. HSP90 expression is shown as a loading control. **(K)** Glucose consumption rates of A549 cells cultured with or without serine and 2 μM FCCP for 72 hours, n=3. Data shown for all panels are means ± SD.

Supplementary Figure 5

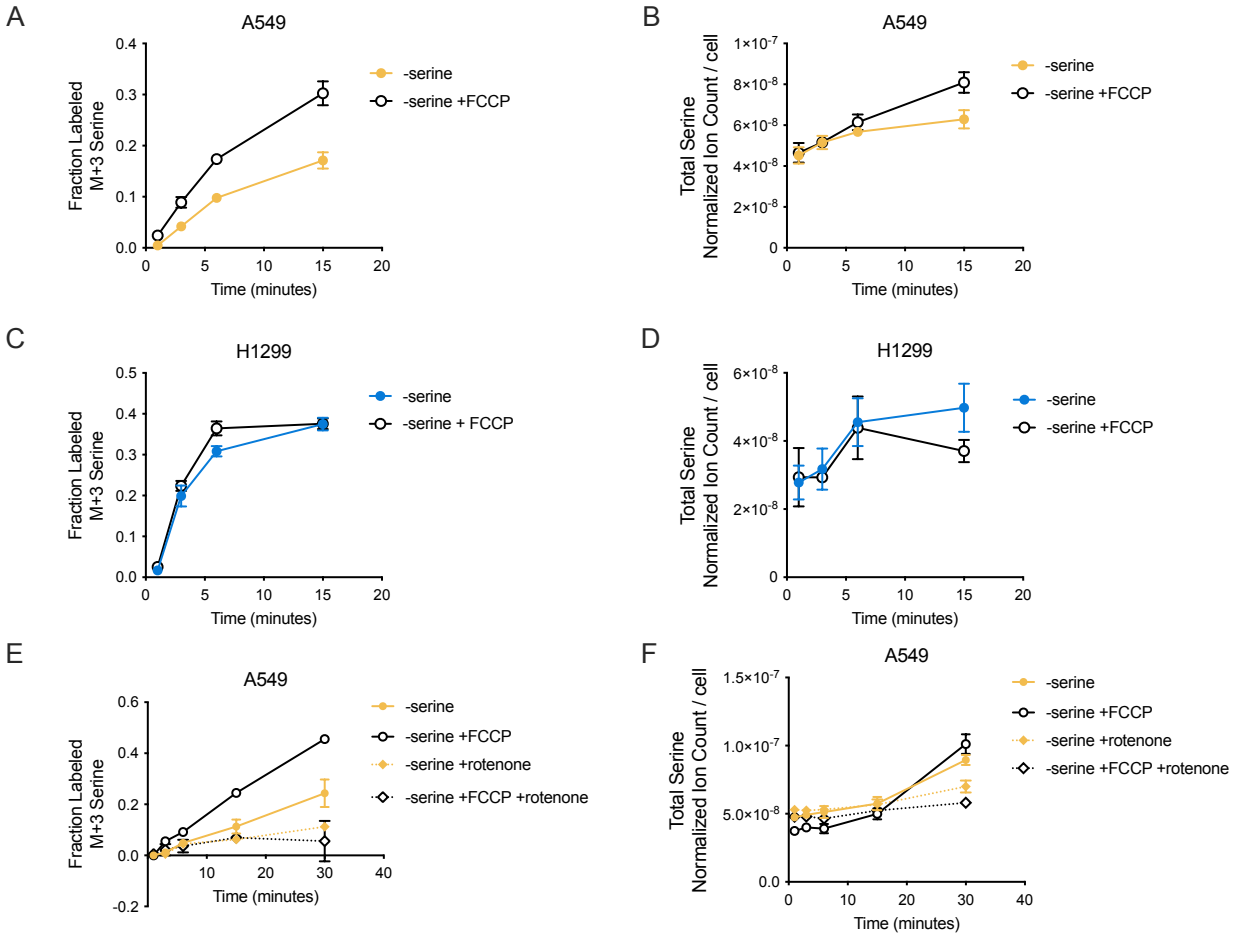

Supplementary Figure 5. Kinetic tracing of labeled carbon from U-^{13}C-glucose into serine following serine withdrawal and FCCP treatment. (A) Fraction of total serine labeled (M+3 serine) from U-^{13}C-glucose over time in A549 cells cultured without serine, and with or without 2 μM FCCP, for 24 hours prior to U-^{13}C-glucose exposure as indicated, n=3. **(B)** Total serine measured in A549 cells cultured without serine and with or without 2 μM FCCP for each time point shown in (A), n=3. **(C)** Fraction of total serine labeled (M+3 serine) from U-^{13}C-glucose over time in H1299 cells cultured without serine and with or without 2 μM FCCP for 24 hours prior to U-^{13}C-glucose exposure as indicated, n=3. **(D)** Total serine measured in H1299 cells cultured without serine and with or without 2 μM FCCP for each time point shown in (C), n=3. **(E)** Fraction of total serine labeled (M+3 serine) from U-^{13}C-glucose over time in A549 cells cultured without serine and with or without 2 μM FCCP and 20 nM rotenone for 24 hours prior to U-^{13}C-glucose exposure as indicated, n=3. **(F)** Total serine measured in A549 cells cultured without serine and with or without 2 μM FCCP and 20 nM rotenone for each time point shown in (E), n=3. All serine measurements were normalized to internal norvaline standard and cell number. Data shown for all panels are means ± SD.

Supplementary Figure 6

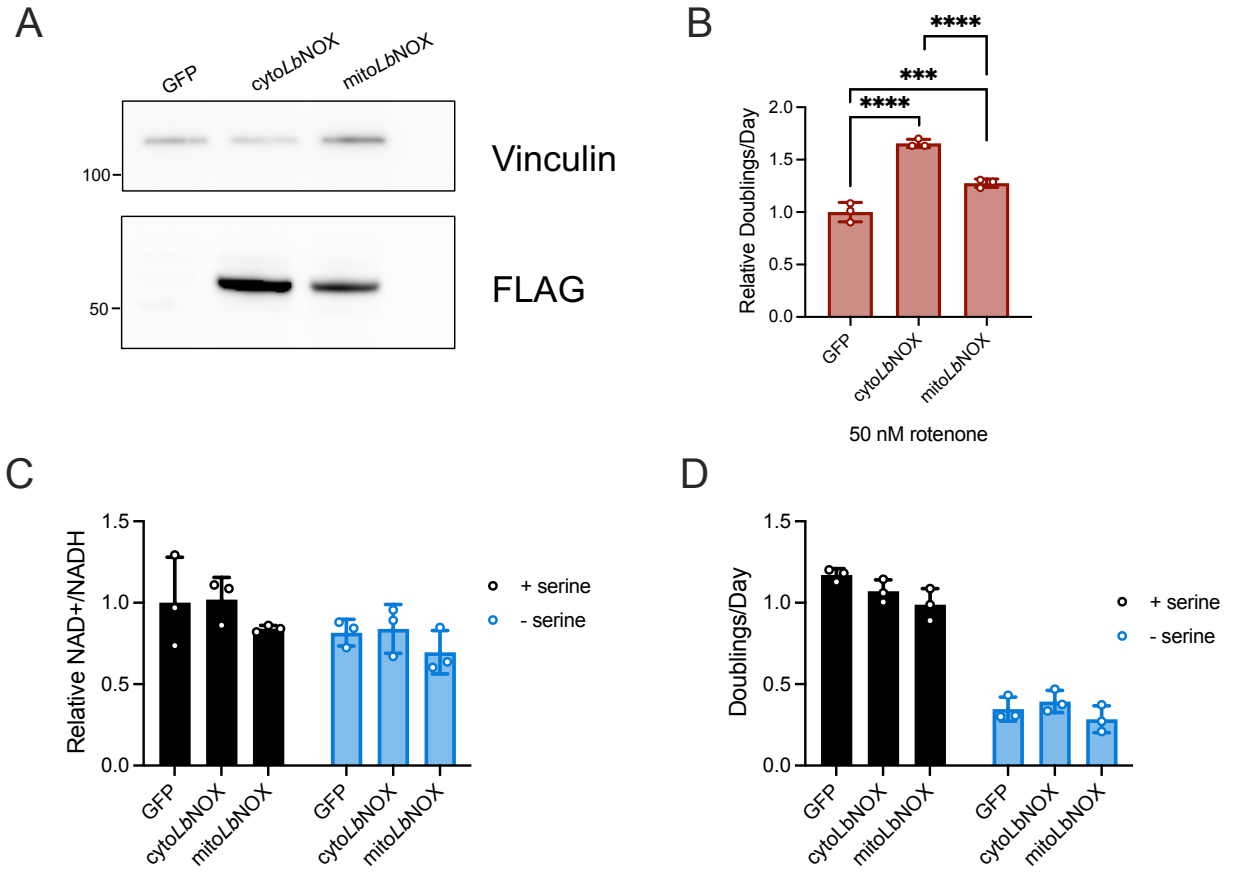

Supplementary Figure 6. Cytosolic or mitochondrial *Lb*NOX expression does not change the cell NAD+/NADH ratio or proliferation of A549 cells cultured without serine. (A) Immunoblot for expression of FLAG-tagged cyto*Lb*NOX or mito*Lb*NOX as indicated. GFP-expressing cells were used as a control. Vinculin expression is shown as a loading control. **(B)** Relative proliferation rate (doublings per day) of A549 cells expressing either cyto*Lb*NOX or mito*Lb*NOX and treated with 50 nM rotenone for 72 hours, n=3. P-values were calculated using one-way ANOVA followed by post-hoc Tukey HSD test, ***p<0.005, ****p<0.001. **(C)** Relative NAD+/NADH ratios of cells expressing either GFP, cyto*Lb*NOX, or mito*Lb*NOX and cultured with or without serine for 24 hours. NAD+/NADH ratios were normalized to the GFP control cells cultured with serine, n=3. **(D)** Proliferation rate (doublings per day) of cells expressing either GFP, cyto*Lb*NOX, or mito*Lb*NOX and cultured with or without serine for 72 hours, n=3. Data shown for all panels are means ± SD.

Supplementary Figure 7

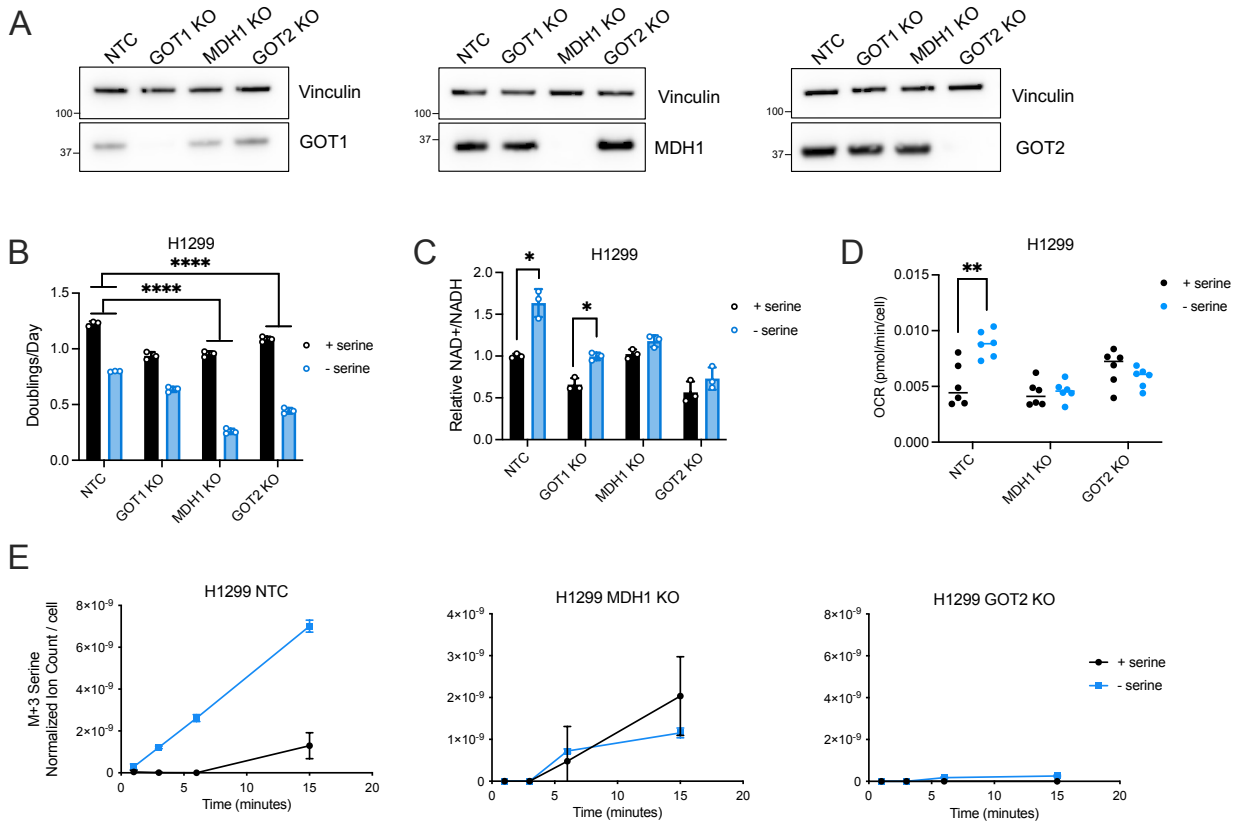

Supplementary Figure 7. MDH1 and GOT2 support the increase in serine synthesis observed in H1299 cells following serine withdrawal. (A) Immunoblots for GOT1 (left), MDH1 (middle), and GOT2 (right) in control cells (NTC, non-targeting control) or cells with knockout (KO) of GOT1, MDH1, or GOT2 as indicated. Vinculin expression is shown as a loading control. **(B)** Proliferation rate (doublings per day) of the indicated cells from (A) cultured with or without serine for 72 hours, n=3. P-values were calculated by nested ANOVA to compare sensitivity to serine depletion between cell lines, ****p<0.001. **(C)** Relative NAD+/NADH ratios of the indicated cells cultured with or without serine for 24 hours, n=3. NAD+/NADH ratios were normalized to H1299 NTC cells cultured with serine. P-values were calculated using unpaired Student's t-test, *p<0.05. **(D)** Oxygen consumption rate (OCR) of the indicated cells cultured with or without serine for 24 hours, n=6. P-values were calculated by unpaired Student's t-test, **p<0.01. **(E)** Serine labeled from U-^{13}C-glucose (M+3) measured over time from the indicated cells cultured with or without serine for 24 hours prior to U-^{13}C-glucose exposure, n=3. Serine levels were normalized to internal standard norvaline and cell number. Data shown for all panels are means ± SD.

Supplementary Figure 8

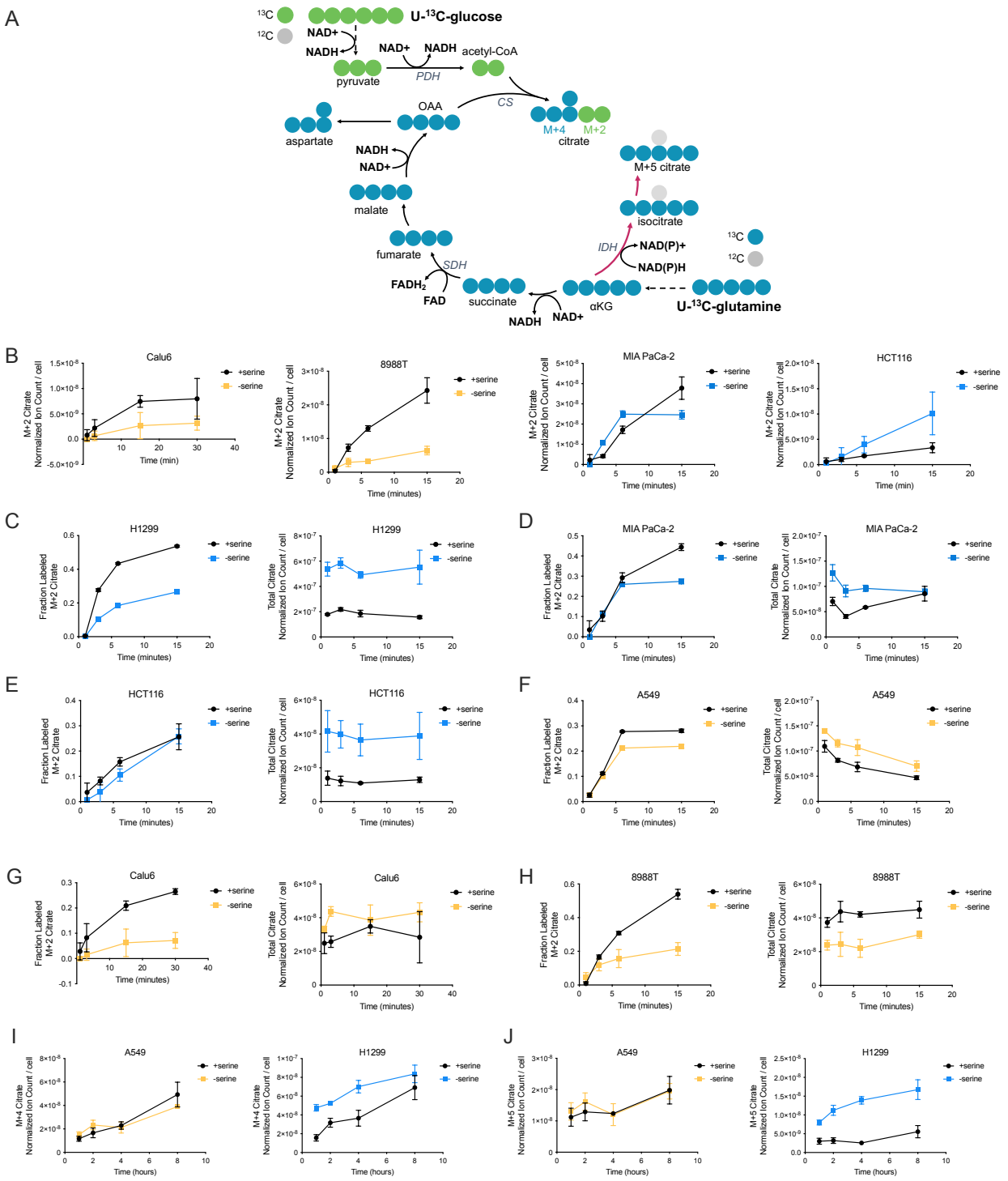

Supplementary Figure 8. Kinetic tracing of labeled carbon from U-^{13}C-glucose and U-^{13}C-glutamine into citrate in cells cultured with or without serine. (A) Schematic depicting isotopically-labeled carbon contribution to citrate from U-^{13}C-glucose and U-^{13}C-glutamine. Abbreviations: PDH – pyruvate dehydrogenase, CS – citrate synthase, IDH – isocitrate dehydrogenase, SDH – succinate dehydrogenase. **(B)** Citrate labeled (M+2) from U-^{13}C-glucose

over time in Calu6, 8988T, MIA PaCa-2, and HCT116 cells cultured with or without serine for 24 hours prior to U-^{13}C-glucose exposure, n=3. **(C-H)** Left of each figure panel: Fraction of citrate labeled (M+2) from U-^{13}C-glucose over time in indicated cells cultured with or without serine for 24 hours, n=3. Right of each figure panel: Total citrate levels in the indicated cells cultured with or without serine for 24 hours for each time point shown in left panel, n=3. **(I)** Citrate labeled (M+4) from U-^{13}C-glutamine over time in A549 and H1299 cells cultured with or without serine for 24 hours, n=3. **(J)** Citrate labeled (M+5) from U-^{13}C-glutamine over time in A549 and H1299 cells cultured with or without serine for 24 hours, n=3. All citrate measurements were normalized to internal norvaline standard and cell number measured in indicated conditions. Data shown for all panels are means ± SD.

Supplementary Figure 9

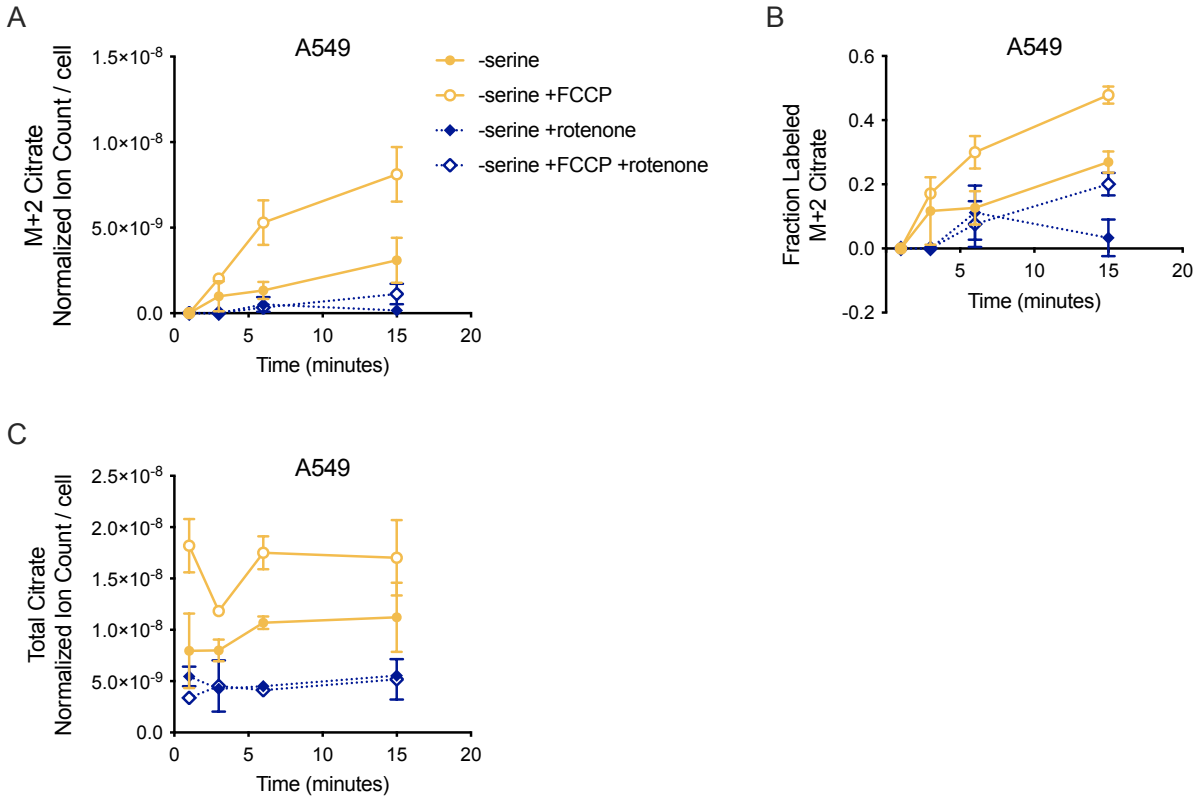

Supplementary Figure 9. Kinetic tracing of labeled carbon from U-^{13}C-glucose into citrate in cells cultured without serine and in the presence or absence of FCCP and/or rotenone. **(A)** Fraction of citrate labeled (M+2) from U-^{13}C-glucose over time in A549 cells cultured without serine for 24 hours, and with or without the addition of 2 μM FCCP or 20 nM rotenone as indicated, n=3. **(B)** Fraction of citrate labeled (M+2) from U-^{13}C-glucose over time in A549 cells cultured without serine for 24 hours, and with or without the addition of 2 μM FCCP or 20 nM rotenone as indicated, n=3. **(C)** Total citrate levels in A549 cells cultured without serine for 24 hours, and with or without the addition of 2 μM FCCP or 20 nM rotenone as indicated, n=3. All citrate measurements were normalized to internal norvaline standard and cell number. Data shown for all panels are means ± SD.

Supplementary Figure 10

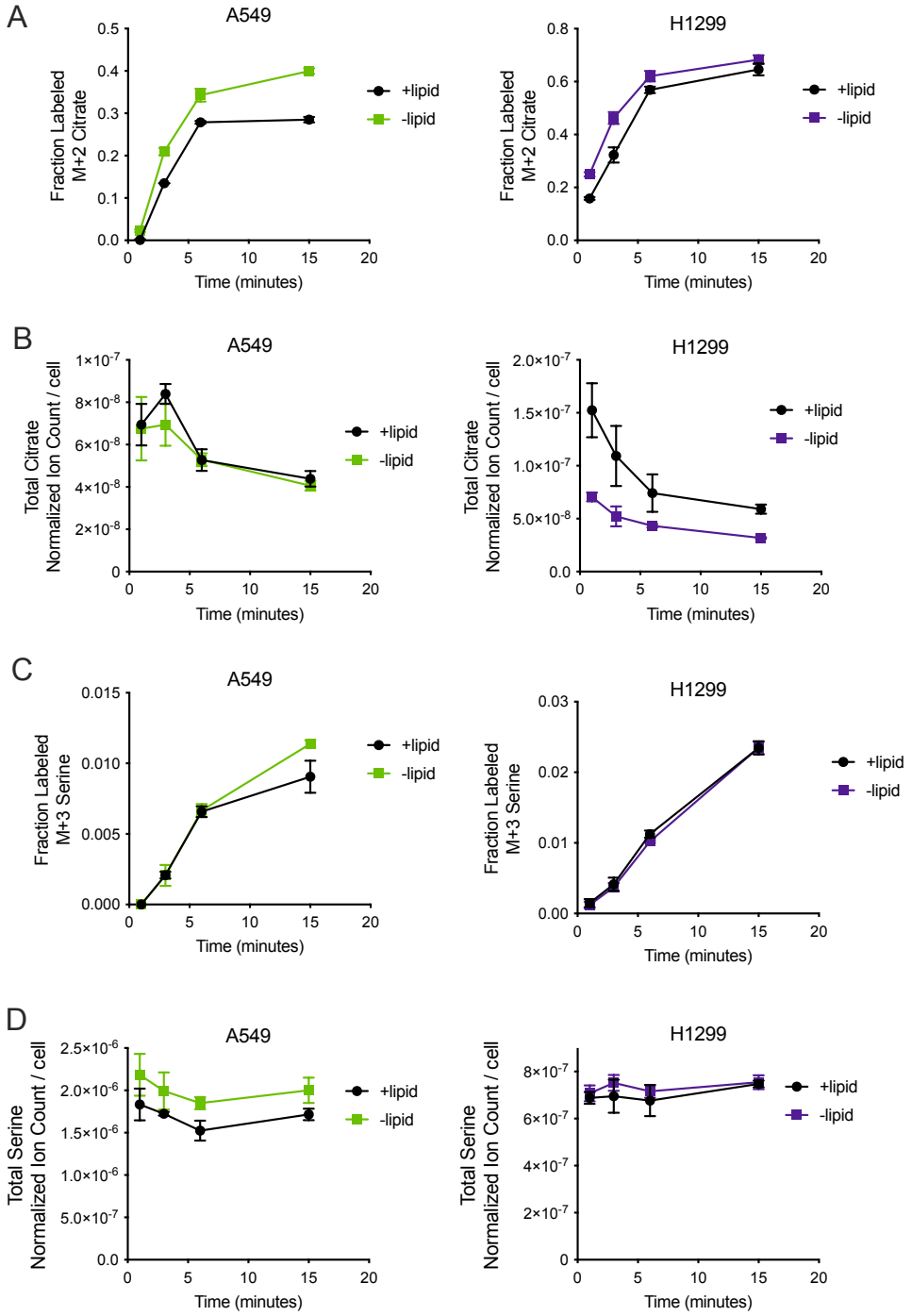

Supplementary Figure 10. Kinetic tracing of labeled carbon from U-^{13}C-glucose into citrate in cells cultured in the presence or absence of lipids. (A) Fraction of citrate labeled (M+2) from U-^{13}C-glucose over time in A549 and H1299 cells cultured with or without lipids for 24 hours as indicated, n=3. **(B)** Total citrate levels in A549 and H1299 cells cultured with or without lipids for 24 hours for each time point shown in (A), n=3. **(C)** Fraction of serine labeled (M+3) from U-^{13}C-glucose over time in A549 and H1299 cells cultured with or without lipids for 24 hours as indicated, n=3. **(D)** Total serine levels in A549 and H1299 cells cultured with or without lipids for

24 hours for each time point shown in (C), n=3. All citrate and serine measurements were normalized to internal norvaline standard and cell number. Data shown for all panels are means ± SD.

Supplementary Figure 11

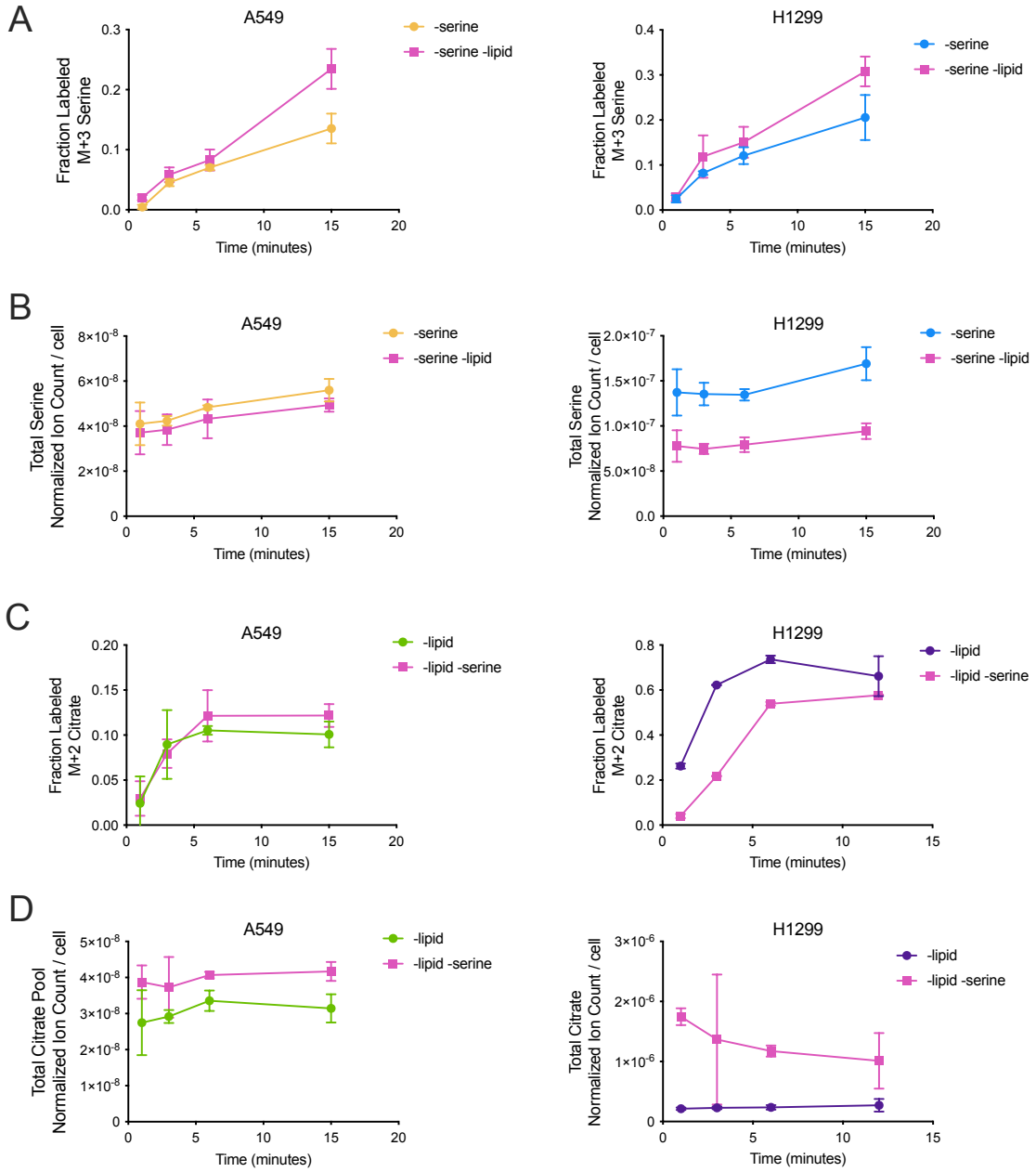

Supplementary Figure 11. Kinetic tracing of labeled carbon from U-^{13}C-glucose into serine and citrate in cells cultured in the absence of serine, lipids, or both serine and lipids. (A) Fraction of serine labeled (M+3) from U-^{13}C-glucose over time in A549 and H1299 cells cultured without serine, and with or without lipids for 24 hours as indicated, n=3. **(B)** Total serine levels in A549 and H1299 cells cultured without serine, and with or without lipids for 24 hours for each time point shown in (A), n=3. **(C)** Fraction of citrate labeled (M+2) from U-^{13}C-glucose over time in A549 and H1299 cells cultured without lipids, and with or without serine for 24 hours as indicated, n=3. (**D)** Total citrate levels in A549 and H1299 cells cultured without lipids, and with or without serine for 24 hours for each time point shown in (C), n=3. All citrate and serine measurements were normalized to internal norvaline standard and cell number. Data shown for all panels are means ± SD.

Supplementary Table 1

Cell Line	Genetic Mutations	Cancer Type	Source
Calu6	Kras Q61K TP53 R196*	Lung Adenocarcinoma	pleural effusion
A549	Kras G12S Stk11 Q37*	Lung Adenocarcinoma	lung
PaTu 8988T	Kras G12V TP53 R282W Smad4 del EP300 del	Pancreatic ductal adenocarcinoma	liver metastasis
MIA PaCa-2	Kras G12C TP53 R248W CDKN2A del	Pancreatic ductal adenocarcinoma	pancreas
H1299	Nras Q61K TP53 del	Lung Adenocarcinoma	lymph node metastasis
HCT116	Kras G13D BRCA2 I2675Dfs CDKN2A mut EP300 mut PIK3CA H1047R PPMID L450* TGFBR2 K128Sfs	Colon Carcinoma	colon
A375	BRAF V600E CDKNA E61* TERTc.1-146C>T	Melanoma	skin
MDA-MB-231	BRAF G464V Kras G13D TP53 R280K CDKN2A/B del TERTc.1-146C>T	Triple Negative Breast Adenocarcinoma	pleural effusion
MCF7	PIK3CA E545K GATA3 D336Gfs CDKN2A del	ER+ HER2- Breast Carcinoma	pleural effusion

Figure 1

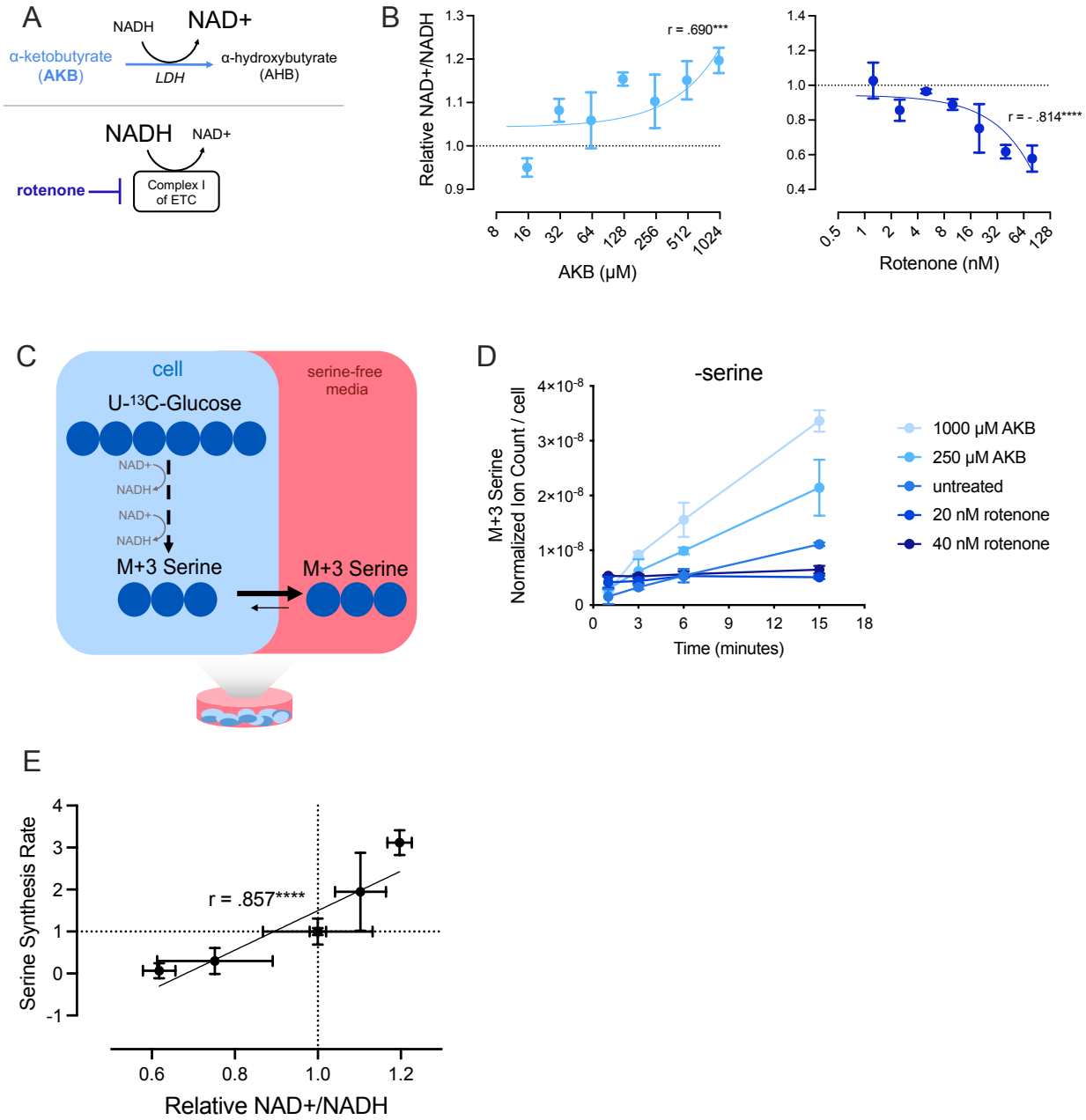
A
NADH
NAD+
α-ketobutyrate
(AKB)
LDH
α-hydroxybutyrate
(AHB)
NADH
NAD+
rotenone
Complex I
of ETC
B
Relative NAD+/NADH
r = .690***
AKB (μM)
r = - .814****
Rotenone (nM)
C
cell
serine-free
media
U-13C-Glucose
NAD+
NADH
NAD+
NADH
M+3 Serine
M+3 Serine
D
-serine
M+3 Serine
Normalized Ion Count / cell
Time (minutes)
1000 μM AKB
250 μM AKB
untreated
20 nM rotenone
40 nM rotenone
E
Serine Synthesis Rate
r = .857****
Relative NAD+/NADH

Figure 2

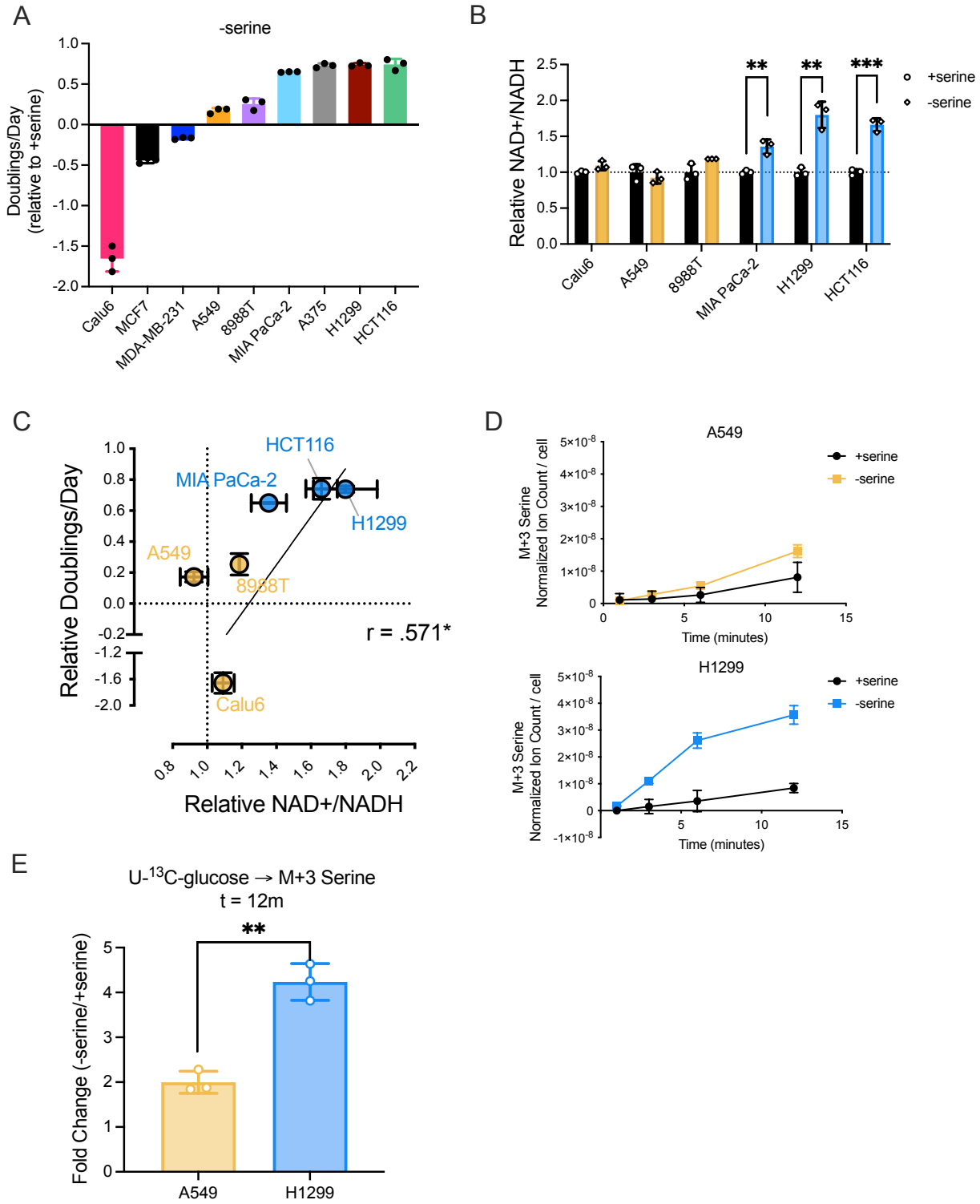
A
-serine
Doublings/Day (relative to +serine)
1.0
0.5
0.0
-0.5
-1.0
-1.5
-2.0
Calu6
MCF7
MDA-MB-231
A549
8988T
MIA PaCa-2
A375
H1299
HCT116
B
Relative NAD+/NADH
2.5
2.0
1.5
1.0
0.5
0.0
**
**
***
+serine
-serine
Calu6
A549
8988T
MIA PaCa-2
H1299
HCT116
C
Relative Doublings/Day
1.0
0.8
0.6
0.4
0.2
0.0
-0.2
-1.2
-1.6
-2.0
HCT116
MIA PaCa-2
H1299
A549
8988T
Calu6
r = .571*
0.8
1.0
1.2
1.4
1.6
1.8
2.0
2.2
Relative NAD+/NADH
D
A549
M+3 Serine Normalized Ion Count / cell
5×10-8
4×10-8
3×10-8
2×10-8
1×10-8
0
+serine
-serine
0
5
10
15
Time (minutes)
H1299
M+3 Serine Normalized Ion Count / cell
5×10-8
4×10-8
3×10-8
2×10-8
1×10-8
0
-1×10-8
+serine
-serine
5
10
15
Time (minutes)
E
U-13C-glucose → M+3 Serine
t = 12m
**
Fold Change (-serine/+serine)
5
4
3
2
1
0
A549
H1299

Figure 3

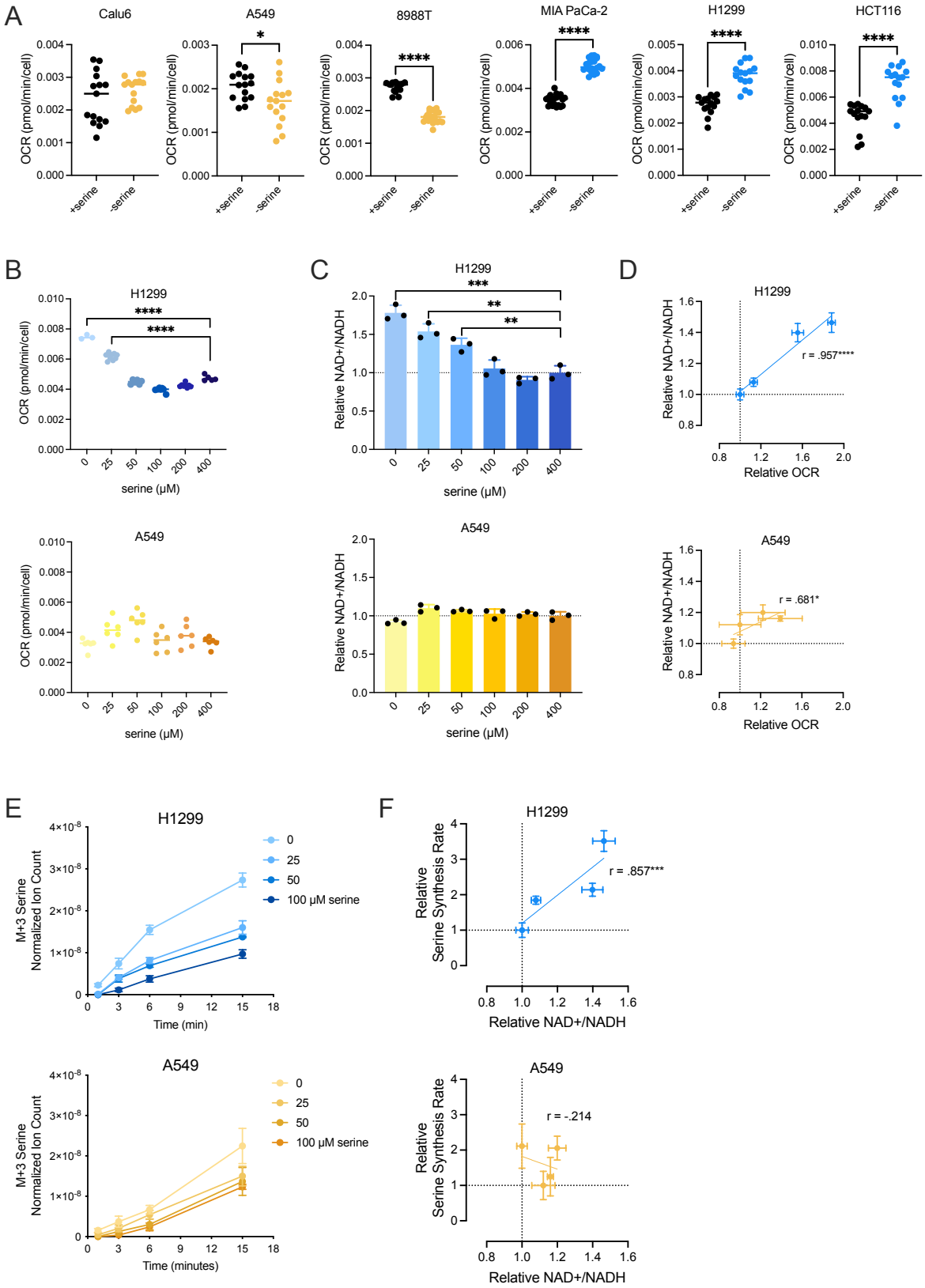
A
Calu6
A549
8988T
MIA PaCa-2
H1299
HCT116
OCR (pmol/min/cell)
+serine
-serine
B
H1299
A549
serine (μM)
C
Relative NAD+/NADH
D
Relative OCR
r = .957****
r = .681*
E
M+3 Serine Normalized Ion Count
Time (min)
Time (minutes)
0
25
50
100 μM serine
F
Relative Serine Synthesis Rate
Relative NAD+/NADH
r = .857***
r = -.214

Figure 4

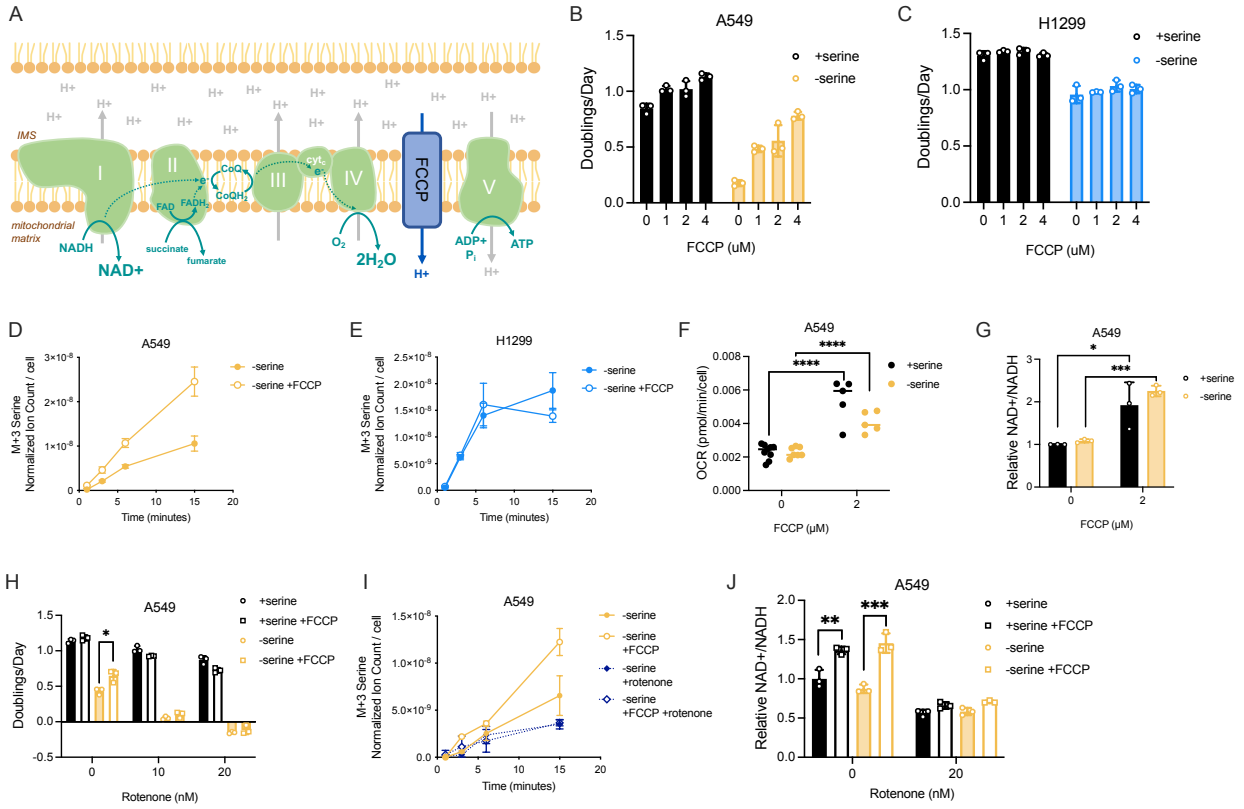
A
IMS
mitochondrial matrix
NADH
NAD+
succinate
fumarate
FAD
FADH2
CoQ
CoQH2
cyt c
O2
2H2O
FCCP
H+
ADP+ Pi
ATP
B
A549
Doublings/Day
+serine
-serine
FCCP (uM)
C
H1299
Doublings/Day
+serine
-serine
FCCP (uM)
D
A549
M+3 Serine Normalized Ion Count / cell
-serine
-serine +FCCP
Time (minutes)
E
H1299
M+3 Serine Normalized Ion Count / cell
-serine
-serine +FCCP
Time (minutes)
F
A549
OCR (pmol/min/cell)
+serine
-serine
FCCP (μM)
G
A549
Relative NAD+/NADH
+serine
-serine
FCCP (μM)
H
A549
Doublings/Day
+serine
+serine +FCCP
-serine
-serine +FCCP
Rotenone (nM)
I
A549
M+3 Serine Normalized Ion Count / cell
-serine
-serine +FCCP
-serine +rotenone
-serine +FCCP +rotenone
Time (minutes)
J
A549
Relative NAD+/NADH
+serine
+serine +FCCP
-serine
-serine +FCCP
Rotenone (nM)

Figure 5

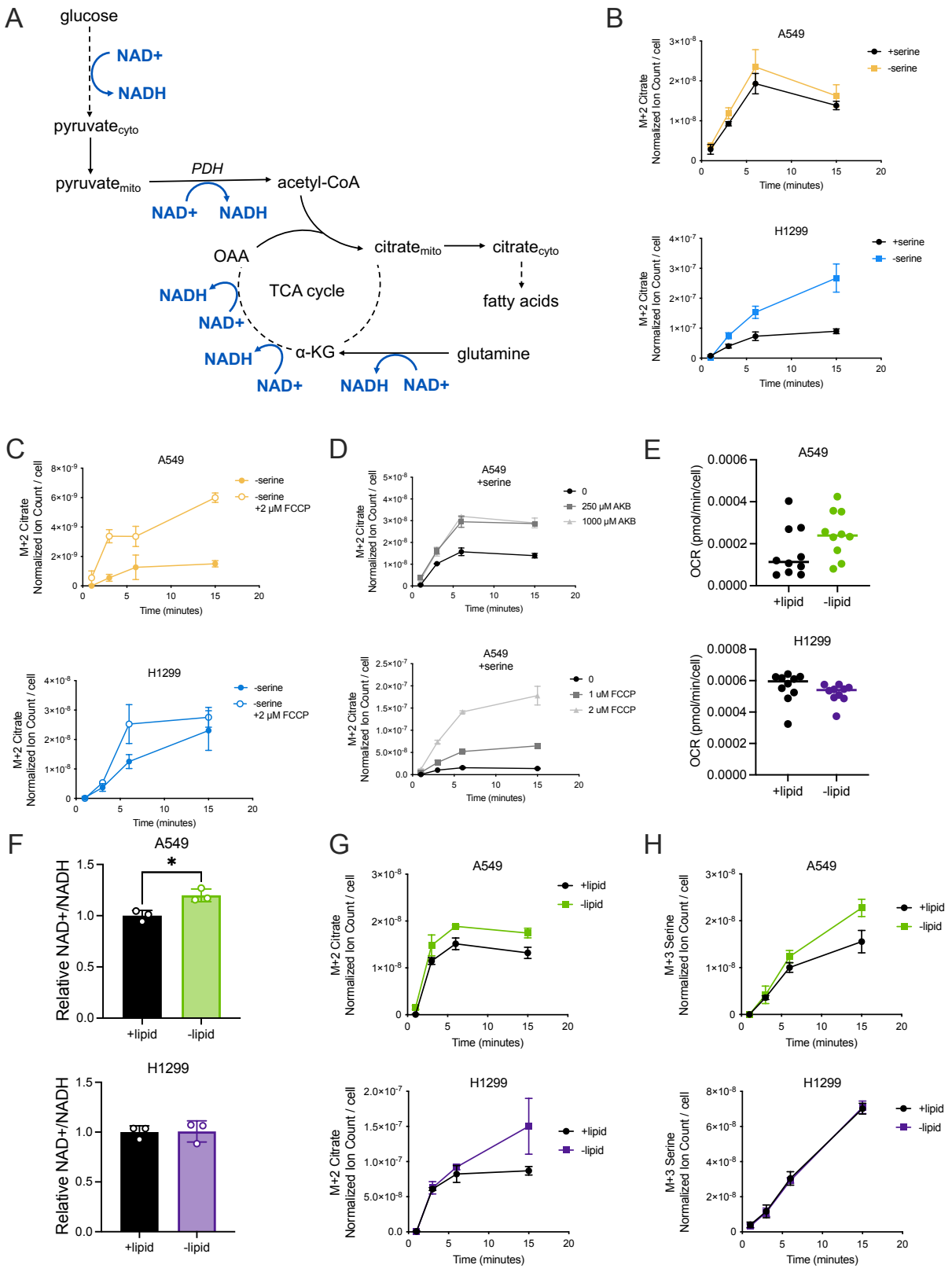
A
glucose
NAD+
NADH
pyruvate$_{cyto}$
pyruvate$_{mito}$
PDH
NAD+
NADH
acetyl-CoA
OAA
citrate$_{mito}$
citrate$_{cyto}$
fatty acids
NADH
NAD+
TCA cycle
NADH
NAD+
α-KG
glutamine
NAD+
NADH
NAD+
B
A549
+serine
-serine
M+2 Citrate Normalized Ion Count / cell
Time (minutes)
H1299
+serine
-serine
M+2 Citrate Normalized Ion Count / cell
Time (minutes)
C
A549
-serine
-serine +2 μM FCCP
M+2 Citrate Normalized Ion Count / cell
Time (minutes)
H1299
-serine
-serine +2 μM FCCP
M+2 Citrate Normalized Ion Count / cell
Time (minutes)
D
A549 +serine
0
250 μM AKB
1000 μM AKB
M+2 Citrate Normalized Ion Count / cell
Time (minutes)
A549 +serine
0
1 uM FCCP
2 uM FCCP
M+2 Citrate Normalized Ion Count / cell
Time (minutes)
E
A549
OCR (pmol/min/cell)
+lipid
-lipid
H1299
OCR (pmol/min/cell)
+lipid
-lipid
F
A549
*
Relative NAD+/NADH
+lipid
-lipid
H1299
Relative NAD+/NADH
+lipid
-lipid
G
A549
+lipid
-lipid
M+2 Citrate Normalized Ion Count / cell
Time (minutes)
H1299
+lipid
-lipid
M+2 Citrate Normalized Ion Count / cell
Time (minutes)
H
A549
+lipid
-lipid
M+3 Serine Normalized Ion Count / cell
Time (minutes)
H1299
+lipid
-lipid
M+3 Serine Normalized Ion Count / cell
Time (minutes)

Figure 6

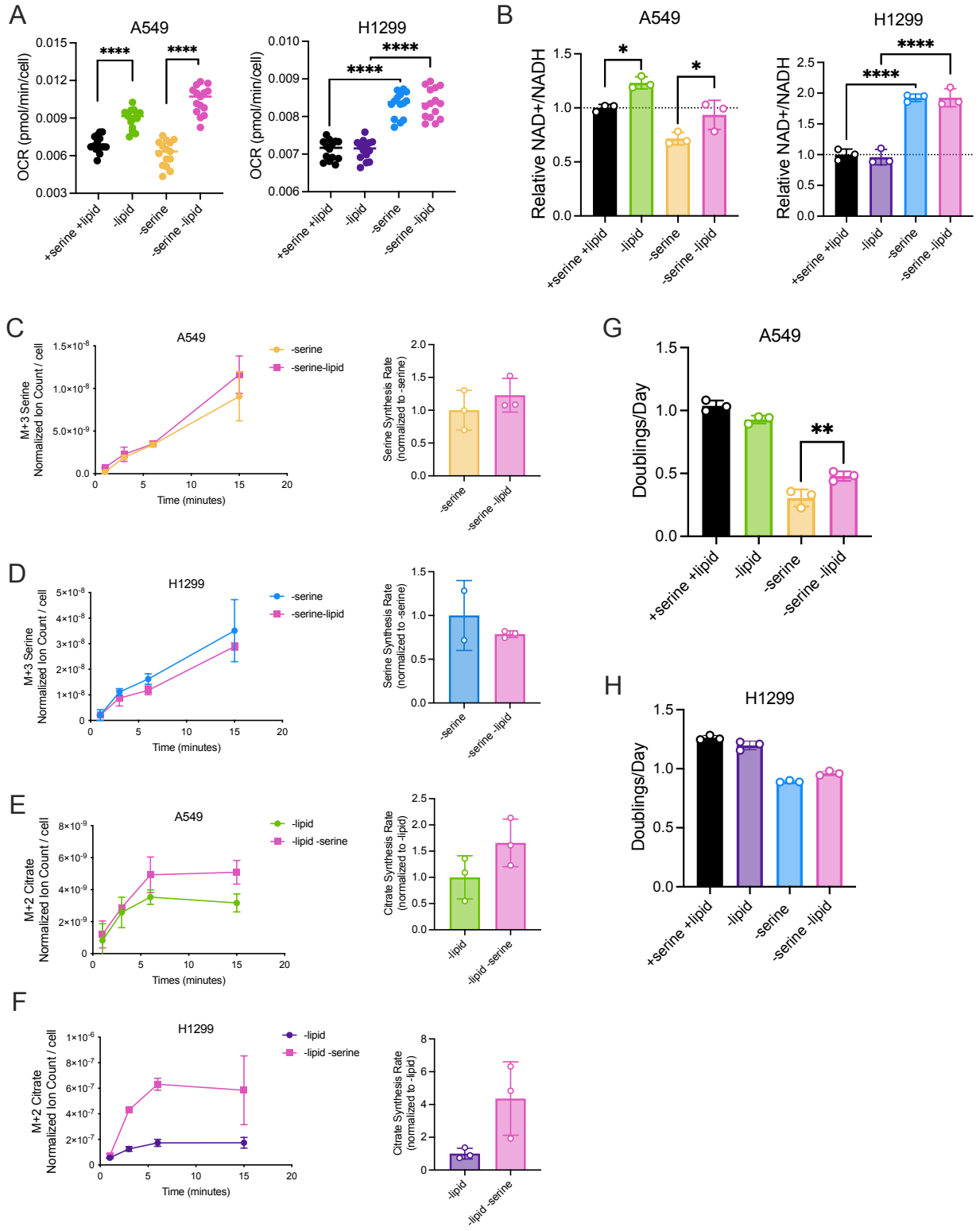
A
A549
H1299
OCR (pmol/min/cell)
****
+serine +lipid
-lipid
-serine
-serine -lipid
B
Relative NAD+/NADH
*
C
M+3 Serine Normalized Ion Count / cell
Time (minutes)
-serine
-serine-lipid
Serine Synthesis Rate (normalized to -serine)
D
E
M+2 Citrate Normalized Ion Count / cell
Times (minutes)
-lipid
-lipid -serine
Citrate Synthesis Rate (normalized to -lipid)
F
G
Doublings/Day
**
H

Figure 7

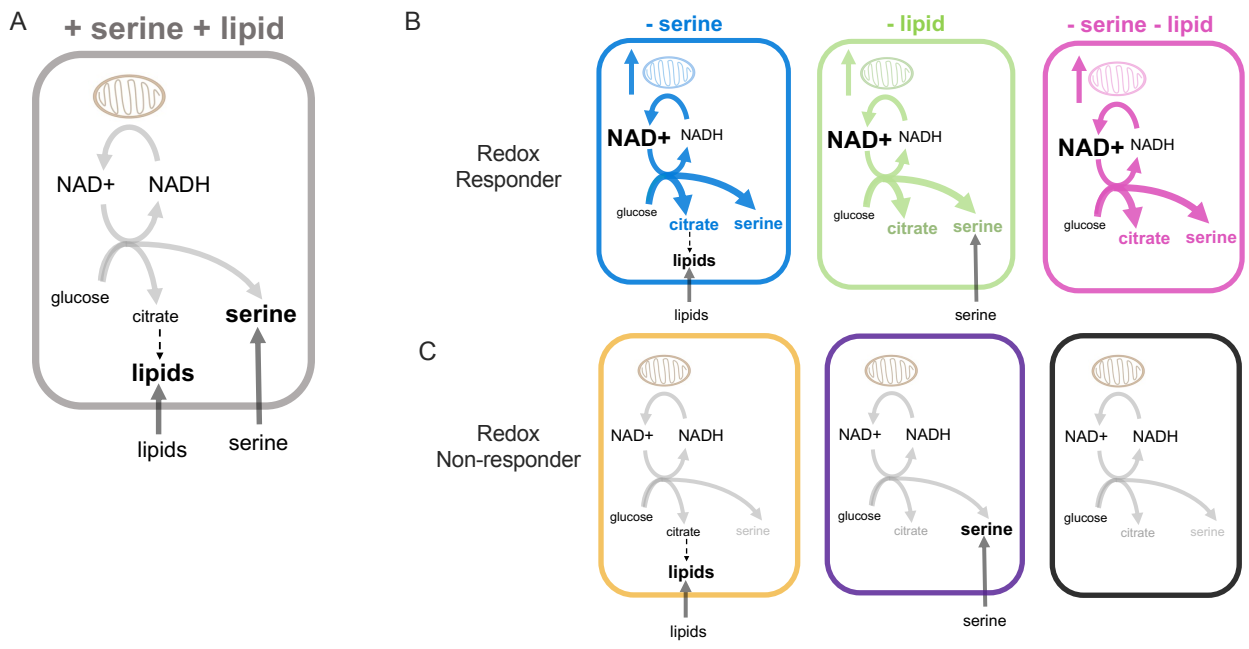
A
+ serine + lipid
NAD+
NADH
glucose
citrate
serine
lipids
lipids
serine
B
- serine
- lipid
- serine - lipid
Redox
Responder
NAD+
NADH
glucose
citrate
serine
lipids
lipids
serine
C
Redox
Non-responder
NAD+
NADH
glucose
citrate
serine
lipids
lipids
serine